Journal Pre-proofs

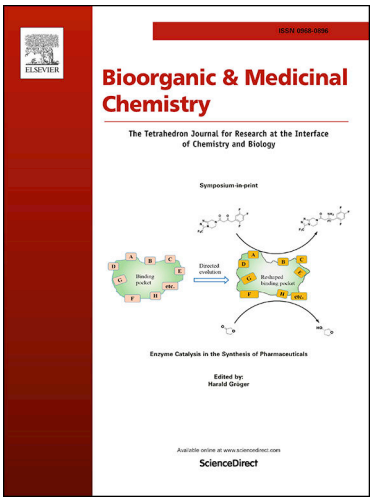

Nitrogen-containing Naringenin Derivatives for Reversing Multidrug Resistance in Cancer

Ricardo J. Ferreira, Mário Gajdács, Annamária Kincses, Gabriella Spengler, Daniel J. V. A. dos Santos, Maria-José U. Ferreira

PII: S0968-0896(20)30628-3
DOI: https://doi.org/10.1016/j.bmc.2020.115798
Reference: BMC 115798

To appear in: *Bioorganic & Medicinal Chemistry*

Received Date: 17 August 2020
Revised Date: 26 September 2020
Accepted Date: 28 September 2020

Please cite this article as: R.J. Ferreira, M. Gajdács, A. Kincses, G. Spengler, D. J. V. A. dos Santos, M.U. Ferreira, Nitrogen-containing Naringenin Derivatives for Reversing Multidrug Resistance in Cancer, *Bioorganic & Medicinal Chemistry* (2020), doi: https://doi.org/10.1016/j.bmc.2020.115798

Graphical **Abstract**

Nitrogen-containing Naringenin Derivatives for Reversing Multidrug Resistance in Cancer

Leave this area blank for abstract info.

Ricardo J. Ferreira[a] Mário Gajdács,[b] Annamária Kincses, [b] Gabriella Spengler, [b] Daniel J. V. A. dos Santos, [b,c]* Maria-José U. Ferreira [a]*

[a] *Research Institute for Medicines (iMed.ULisboa), Faculty of Pharmacy, Universidade de Lisboa, Av. Prof. Gama Pinto, 1649-003 Lisbon, Portugal*

[b] *Department of Medical Microbiology and Immunobiology, Faculty of Medicine, University of Szeged, Dóm tér 10, H-6720 Szeged, Hungary*

[c] *LAQV@REQUIMTE/Department of Chemistry and Biochemistry, Faculty of Sciences, University of Porto, Rua do Campo Alegre, 4169-007 Porto, Portugal*

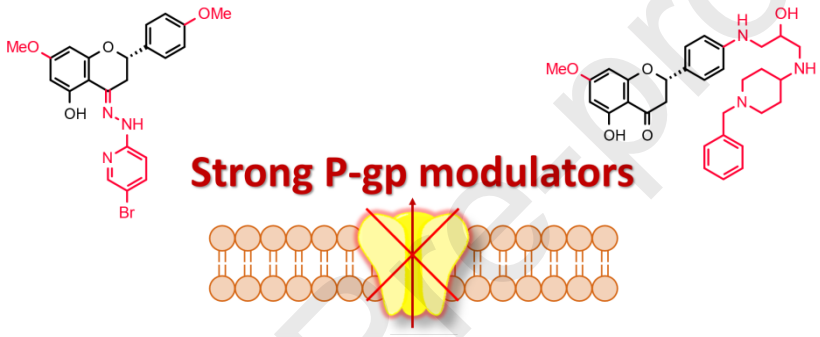

ELSEVIER

Bioorganic & Medicinal Chemistry
journal homepage: www.elsevier.com

Nitrogen-containing Naringenin Derivatives for Reversing Multidrug Resistance in Cancer

Ricardo J. Ferreira,[a] Mário Gajdács,[b] Annamária Kincses,[b] Gabriella Spengler,[b] Daniel J. V. A. dos Santos,[b,c] * Maria-José U. Ferreira [a] *

[a] *Research Institute for Medicines (iMed.ULisboa), Faculty of Pharmacy, Universidade de Lisboa, Av. Prof. Gama Pinto, 1649-003 Lisbon, Portugal*
[b] *Department of Medical Microbiology and Immunobiology, Faculty of Medicine, University of Szeged, Dóm tér 10, H-6720 Szeged, Hungary*
[c] *LAQV@REQUIMTE/Department of Chemistry and Biochemistry, Faculty of Sciences, University of Porto, Rua do Campo Alegre, 4169-007 Porto, Portugal*

ARTICLE INFO

Article history:
Received
Received in revised form
Accepted
Available online

Keywords:
Multidrug resistance
P-glycoprotein
Flavonoids
Efflux modulators
Molecular Dynamics
Docking

ABSTRACT

Naringenin (**1**), isolated from *Euphorbia pedroi*, was previously derivatized yielding compounds **2-13**. In this study, aiming at expanding the pool of analogues of the flavanone core towards better multidrug resistance (MDR) reversal agents, alkylation reactions and chemical modification of the carbonyl moiety was performed (**15-39**). Compounds structures were assigned mainly by 1D and 2D NMR experiments. Compounds **1-39** were assessed as MDR reversers, in human *ABCB1*-transfected mouse T-lymphoma cells, overexpressing P-glycoprotein (P-gp). The results revealed that *O*-methylation at C-7, together with the introduction of nitrogen atoms and aromatic moieties at C-4 or C-4', significantly improved the activity, being compounds **27** and **37** the strongest P-gp modulators and much more active than verapamil. In combination assays, synergistic interactions of selected compounds with doxorubicin substantiated the results. While molecular docking suggested that flavanone derivatives act as competitive modulators, molecular dynamics showed that dimethylation promotes binding to a modulator-binding site. Moreover, flavanones may also interact with a vicinal ATP-binding site in both nucleotide-binding domains, hypothesizing an allosteric mode of action.

1. Introduction

Multidrug resistance (MDR) to anticancer agents is a major concern in chemotherapeutic regimens worldwide. As typical MDR is often related with the over-expression of promiscuous efflux pumps from the ABC transporter superfamily at the surface of cancer cells, the development of small molecules able to impair drug efflux by such transporters is one of the most promising approaches to tackle MDR in cancer.[1,2] Since the modulation of P-glycoprotein (P-gp/ABCB1) by verapamil in P388 cells,[3] several classes of efflux modulators, subdivided in at least three generations, were designed and evaluated,[4] but while reaching clinical trials, none was still approved for clinical usage. Therefore, the continuous exploitation of new scaffolds, able to inhibit one or all members of the efflux triad (P-gp, multidrug-resistance protein 1 – MRP1/ABCC1 – and breast cancer resistance protein – BCRP/ABCG2) is of the utmost importance to understand which chemical moieties are related with the experimentally observed modulatory effects.[5]

Flavonoids are among the compounds already described as efflux modulators, inhibiting all major contributors in MDR.[6] In a previous study by the authors, the flavanone core of naringenin (**1**), isolated in large amounts from the Portuguese endemic species *Euphorbia pedroi*, was chemically modified at position C-4 to render imines **2-13** (Figure 1).[7] Promising results were obtained for naringenin derivatives **2-8**, which exhibited high MDR reversal activity towards BCRP, and **9-12** that were selective efflux modulators of MRP1 (Figure 1).[7]

Therefore, in this study, aiming at obtaining derivatives with improved P-gp modulating activity, further modifications of the flavanone core, namely *O*-methylation reactions followed by condensation of the ketone group at C-4 with different amine derivatives or the introduction of a propanolamine moiety at ring B, gave rise to twenty-five additional naringenin derivatives. This new library of compounds (**14-39**), along with compounds **2-13**, were investigated for their ability to modulate P-gp, using as model human *ABCB1*-transfected mouse T-lymphoma (L5178Y-MDR) cells. The cytotoxicity of the compounds was assessed in the same cell line. Moreover, the MDR reversal activity of compounds **23**, **31** and **37** was additionally evaluated in combination with the anticancer drug doxorubicin to identify potential synergistic effects. Finally, and aiming at obtaining further insights into the structural basis related to efflux modulation by the herein prepared flavanone derivatives, *in silico* approaches were undertaken to clarify the specific role of methylation on the observed MDR-reversal activity.

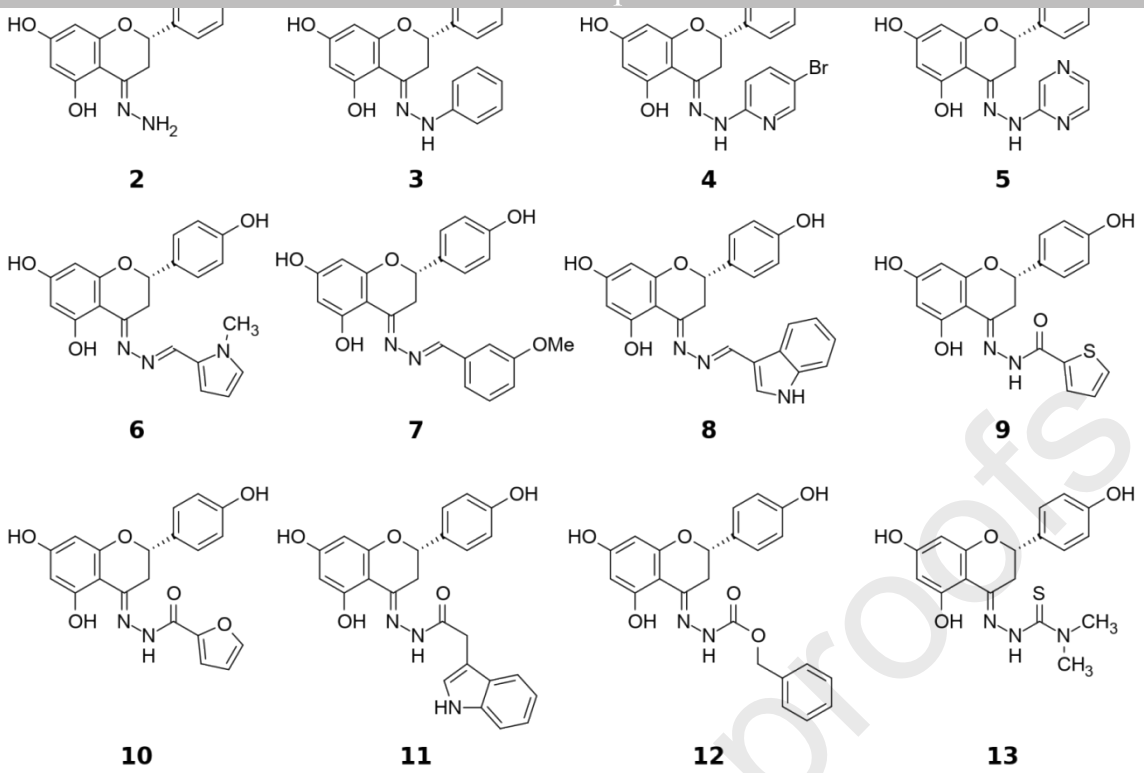

Figure 1. Naringenin derivatives **2**-**13**.

2. Results and Discussion

In a previous study a large amount of naringenin (**1**) was isolated from *Euphorbia pedroi*, from which compounds **2**-**13** were obtained, by chemical modification of the flavanone scaffold at C-4, and assessed as P-gp, MRP1 and BCRP modulators (Figure 1).[7]

2.1. Preparation of naringenin (1) derivatives

To generate a wider pool of derivatives, in the present study the methylation of the phenolic hydroxyls at C-7 and C-4´ with dimethyl sulfate (Scheme 1, i) was performed to yield 7-methoxy-naringenin (sakuranetin, **14**) and 7,4'-dimethoxy-naringenin (4'-methoxysakuranetin, **24**) as alternative building blocks to naringenin (**1**). Following, condensation of the carbonyl group at C-4 of compounds **14** and **24** with different amine derivatives allowed the preparation of *O*-mono- (**15**-**23**) and *O*-dimethylated (**25**-**31**) imines (C=N-NH-R) (Scheme 1, ii).

When comparing the ^{1}H and ^{13}C NMR data of compounds **14** and **24** with those of naringenin (**1**), new signals were found for each methoxy group at C-7 (δ_H 3.85; δ_C 56.2 ppm) and C-4' (δ_H 3.86; δ_C 55.6 ppm). The ^{1}H NMR/^{13}C NMR data of compounds **15**-**23** and **25**-**31** were then assigned by comparing with those of the parent compounds (**14**, **24**). Thus, and besides the extra signals assigned to the new imine moiety, the major differences were observed for the ^{13}C NMR data, namely at C-4 where, as expected, the signal of the carbonyl function of the parent compounds (δ_C 197.6 and δ_C 197.5 ppm of **14** and **24**, respectively) undertook a strong diamagnetic effect, resonating between δ_C 150.8 - 167.3 ppm.

Another approach for the development of flavanone-based P-gp efflux modulators was the introduction of primary or secondary amines at the position C-4' of the flavanone core (Scheme 2), following the initial studies by Chiba and co-workers in propafenones.[8,9] Accordingly, after *O*-methylation of compound **1** at C-7 (Scheme 1, i), the reaction of compound **14** with epichlorohydrin at C-4' yielded compounds **32** and **33** (Scheme 2, i), which followed by treatment with amines yielded the corresponding propanolamines (Scheme 2, ii, compounds **34**-**37**). Derivatives **38** and **39** were also prepared by reaction of **32** (or **33**) with indole or thiophenol, respectively.

The introduction of the oxyran-2-yl moiety of compound **32** was substantiated by the appearance of three additional signals in the ^{13}C NMR spectrum, corresponding to one oxymethylene linked to the oxygen at C-4' (δ_C 70.2) and two other carbon signals (δ_C 44.4 and 50.6 ppm) from the oxyrane ring. The secondary product, 4'-(3-chloro-2-hydroxy propoxy)-7-methoxy-naringenin (Scheme 2, **33**), obtained as a side reaction owing to the opening of the epoxide ring, was evidenced by a strong paramagnetic effect on the oxymethine group ($\Delta\delta_H$ = 4.22; δ_C 70.0) associated with the presence of the chlorine atom. Reaction of **32** (or **33**) with a selected amine yielded compounds **34**-**37**, all containing a new propanolamine moiety. Additionally, reactions with indole and thiophenol yielded compounds **38** and **39**. When comparing the ^{13}C NMR spectra of compounds **34**-**39** with that of compound **32**, along with the new signals corresponding to the amine moiety, paramagnetic effects in the ^{13}C NMR signals at C-6' ($\Delta\delta_C$ = + 13.7 – 19.5 ppm) and C-7' ($\Delta\delta_C$ = + 2.4 – 16.9 ppm) were additionally observed.

2.2. Cytotoxic Activities

The cytotoxicity of compounds **1**-**39** was evaluated on L5178Y parental (L5178Y-PAR) and human *ABCB1*-gene transfected (L5178Y-MDR) mouse T-lymphoma cells, through the MTT assay. The half maximal inhibitory concentration (IC_{50}) for each compound was calculated by fitting the dose-dependent curves. Excepting compounds showed in Table 1, no relevant cytotoxicity was found for most of the derivatives (*Supporting*

Info ...non-

compounds **28** and **31** were more cytotoxic against resistant cells. Furthermore, when analyzing the cytotoxic activity data of all compounds (*Supporting Information*, Tables S1 and S2), it could ...methylated to *O*-mono- and *O*-dimethylated compounds, having identical moieties at position C-4 (**4**, **17** and **27**; **10**, **21** and **29**; **11**, **22** and **30**; and **12**, **23** and **31**).

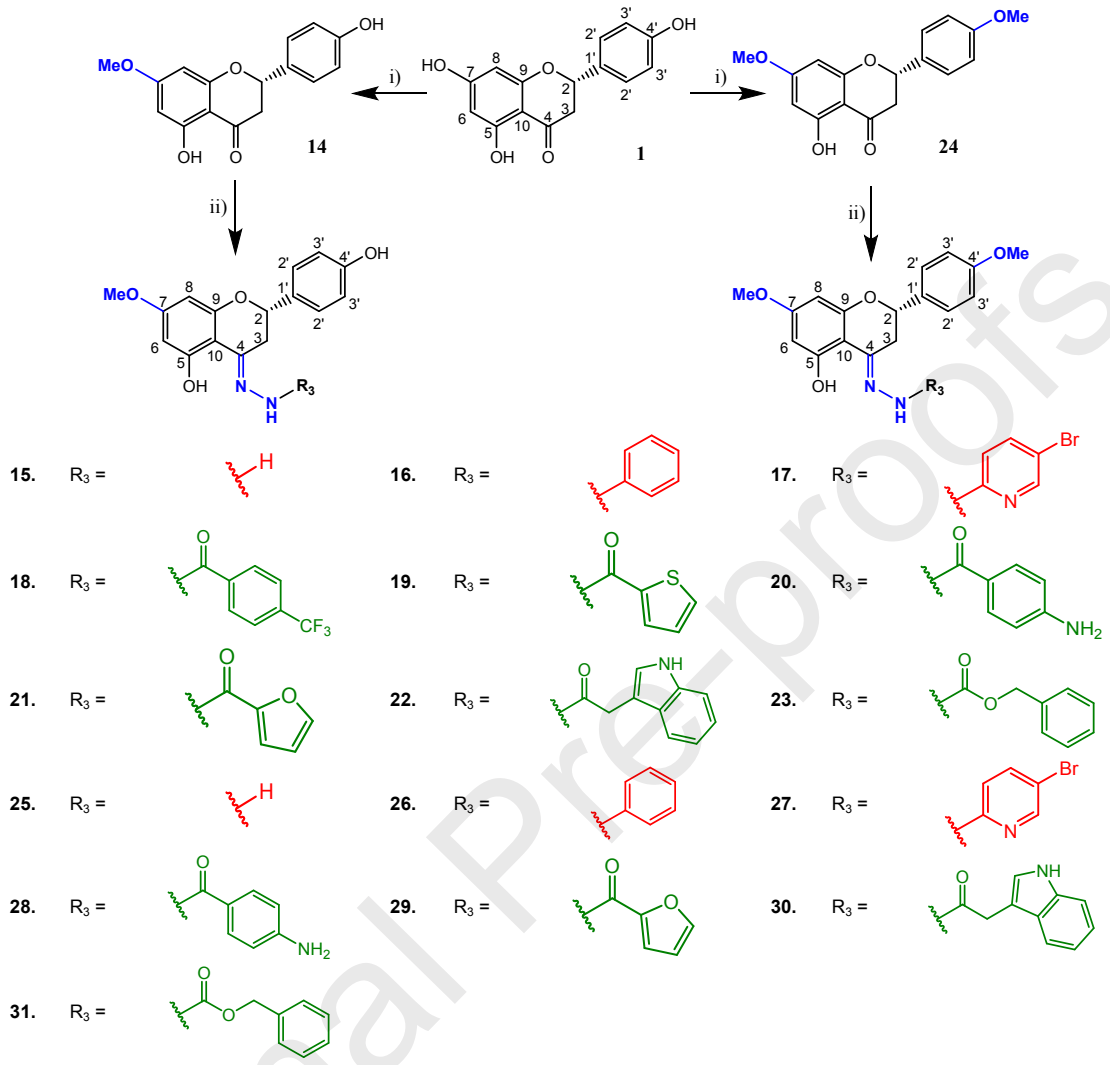

Scheme 1. Preparation of *O*-monomethylated and *O*-dimethylated naringenin (**1**) derivatives (**15**–**31**). Reagents and conditions: (i) DMS (1 eq.) and K_2CO_3 (1 eq.) in acetone, 50 ºC, 12 h; (ii) hydrazine (R-NH-NH_2) or carbohydrazide (R-CO-NH-NH_2) (2.0 eq.) in ethanol, reflux, 12-80 h.

Table 1. Cytotoxic activity of compounds (IC_{50} < 10 μM) on parental (L5178Y-PAR) or ABCB1-transfected (L5178Y-MDR) mouse T-lymphoma cells.[a]

Compounds	L5178Y-PAR	L5178Y-MDR
17	4.3 ± 1.0	12.7 ± 1.0
19	9.4 ± 1.1	12.0 ± 1.1
27	8.0 ± 1.1	10.7 ± 1.1
28	3.9 ± 1.2	1.3 ± 1.1
29	2.7 ± 1.2	3.4 ± 1.2
30	8.6 ± 1.1	7.5 ± 1.1
31	> 100	7.2 ± 1.4
35	9.3 ± 1.1	17.4 ± 1.3

[a] No relevant cytotoxicity was found for the remaining compounds (IC_{50}'s ranging from 11.3 ± 1.2 to > 100 μM, Tables S1 and S2).

2.3. Modulation of P-glycoprotein Efflux

The ability of compounds **1**-**39** to act as efflux modulators was evaluated on parental mouse T-lymphoma cell line (L5178Y-PAR) and in its corresponding MDR subline (L5178Y-MDR), overexpressing P-gp, through the Rhodamine-123 (R123) accumulation assay, by flow cytometry. The fluorescence activity ratio (FAR) was measured to assess the intracellular accumulation of R123 in the cells. Verapamil was used as positive control (20 μM). The compounds were evaluated at 2 μM and 20 μM. Compounds with FAR values greater than 1 were considered as active P-gp modulators and those with FAR > 10 as strong modulators.

When analyzing FAR values obtained for the set **2**-**31** (Table 2) at 20 μM, most of the compounds were found to be moderate (FAR 1.10 – 8.80) to strong (FAR 11.08 – 67.24) P-gp modulators. At this concentration, the *O*-monomethylated compound **23**, bearing an imine substituent at C-4 with a benzyloxy moiety, showed the highest reversing activity (FAR

= 67 FAR 9.66, at 20 µM). Very strong FAR values (> 40) were also found for compounds **5**, **16**, **17**, and **22**. However, compound **27**, also *O*-dimethylated and having an imine substituent with a = 10.67 and 30.54, at 2 and at 20 µM, respectively), inhibiting the transport of rhodamine123 by P-gp at larger extent than verapamil at 20 µM

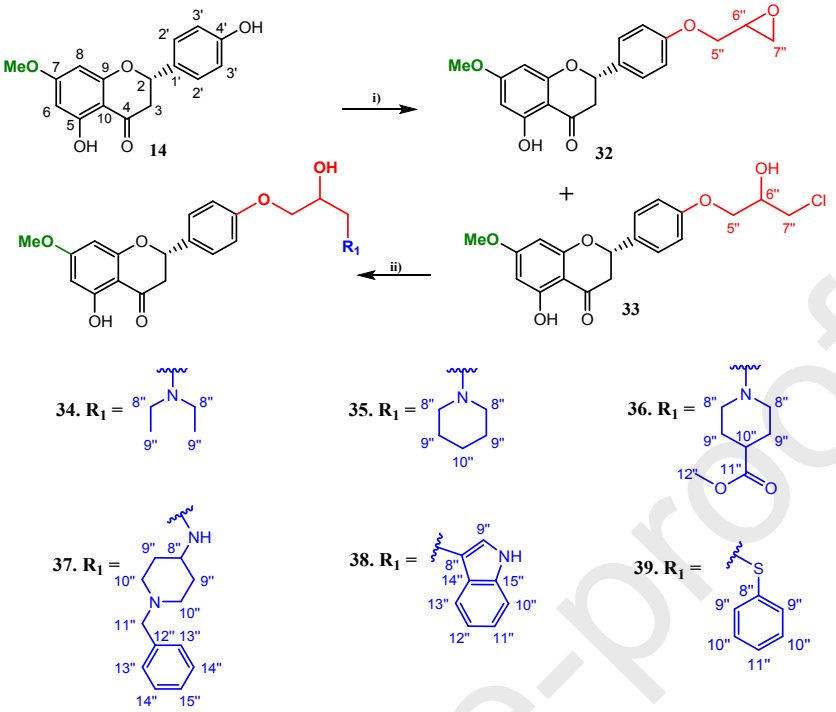

Scheme 2. Preparation of sakuranetin (**14**) derivatives at position C-4' (**32-39**). Reagents and conditions: (i) epichlorohydrin (1.5 eq.) in ethanol and NaOH (1.1 eq.), reflux, overnight; (ii) amine/thiophenol (1.0 equiv.) in MeOH, catalytic amount of acetic acid, reflux, 24-48 h. Compounds **32** and **33** were obtained in 3:1 ratio.

As it can be observed in Table 2, *O*-methylation of C-7 (**14**) and C-4' (**24**) alone and the substitution of the ketone function by the simplest hydrazone moiety (=N-NH_2) (**2**, **15** and **25**), excepting for compound **15** (FAR = 15.60 at 20 µM), did not improve significantly the MDR reversal activity. Conversely, a strong increase of the activity was found for several compounds having new imine moieties at C-4. The data suggests that unsubstituted phenyl rings (**16**, **23** and **26**), heterocyclic rings (**5**, **17** and **27**) and indoles (**22** and **30**) are the most important for increasing the MDR-reversal activity of flavanone derivatives.

In turn, as it can be observed in Table 3, in the set of compounds resulting from alkylation of the hydroxyl group at C-4' (**32-39**), a strong increase in the activity was observed for the propanolamine derivatives (**34-37**), when comparing with the starting compounds, naringenin (**1**) or sakuranetin (**14**). The most active compound was **37**, which was found to be a very strong modulator (FAR = 18.70 and 62.09, at 2 and 20 µM, respectively), being two- and six-fold, more active than verapamil at the highest concentration. Strong activity was also found at 20 µM for compounds **34-36** with FAR values ranging from 30.76 (**35**) to 43.68 (**36**). Conversely, compounds **38** and **39**, with indole and thiophenol substituents, exhibited lower activity (Table 3).

In the set of compounds **34-37**, through the analysis of log*P* and pKa, two of the most important physico-chemical properties that are directly related with the ability to modulate P-gp efflux [8,10], it was possible to verify that while the MDR reversal activity at lower concentration seems to be correlated with the presence of a nitrogen (**34-36**), the presence of both a nitrogen together with an additional aromatic moiety (**37**) seems to further improve the potency of the P-gp efflux modulator (FAR 18.70 at 2 µM). As previously demonstrated for tariquidar,[11] such features are expected to promote a more elongated conformation that favors membrane permeation.

2.4. Combination Assay with the Anticancer Drug Doxorubicin

For investigating the type of *in vitro* interaction with the clinical antitumor drug doxorubicin, two representatives of the most active compounds in the R123 functional assay, from both C-4 (**23**), and C-4' (**37**) series, were evaluated in a combination chemotherapy model in resistant mouse T-lymphoma cells (L5178Y-MDR). Compound **31**, which was found to be more cytotoxic against MDR cells in the cytotoxicity assay, was additionally included. The extent of interaction between doxorubicin, a known P-gp substrate, and the compounds was calculated by the Chou-Talalay method, by using the combination index (CI).[12] The combination index is estimated from the multiple drug effect equation, derived from the median-effect principle of the mass-action law, and provides quantitative determination for synergism (CI < 1), additive effect (CI = 1) and antagonism (CI > 1). It takes into account both the potency and the shape of the dose-effect curve of each drug alone and their combination.[12,13] Thus, any compound able to inhibit P-gp is expected to potentiate cytotoxic effects when co-administered with any given anticancer drug.

As it can be observed in Table 4, both P-gp modulators tested displayed synergism (**23**) (0.3 < CI < 0.7) or strong synergism (**37**) (0.1 < CI < 0.3), enhancing the cytotoxicity of

doxo
substantiating their anti-MDR potential. In turn, compound **31**, which did not modulate P-gp efflux activity on the transport assay, was able to improve the cytotoxicity of doxorubicin synergistically, suggesting that it acts with a different mechanism for re-sensitizing the MDR phenotype.

Table 2. Effect of naringenin and derivatives (**1**-**31**) on P-gp mediated R123 efflux, in *ABCB1*-transfected murine T-lymphoma (L5178Y-MDR) cells.

		Fluorescence Activity Ratio (FAR)				Fluorescence Activity Ratio (FAR)	
		2 µM	20 µM			2 µM	20 µM
Parent	**1**	0.72	0.72	*O*-monomethylated	**15**	1.26	15.60
	14	1.06	1.32		**16**	1.16	40.31
	24	1.03	1.36		**17**	2.10	64.70
Non-methylated	**2**	0.72	3.13		**18**	0.83	2.55
	3	1.16	4.86		**19**	1.39	1.54
	4	1.08	26.80		**20**	0.96	1.10
	5	1.65	47.00		**21**	1.28	11.08
	6	0.64	6.54		**22**	1.12	40.64
	7	0.78	13.58		**23**	4.14	67.24
	8	0.95	17.71	*O*-dimethylated	**25**	0.85	1.06
	9	0.92	1.13		**26**	1.80	13.79
	10	0.86	0.94		**27**	10.67	30.54
	11	1.00	2.48		**28**	1.32	18.88
	12	0.76	8.80		**29**	2.24	18.47
	13	2.17	23.04		**30**	2.47	26.93
DMSO (2%)			1.01		**31**	0.94	1.13
Verapamil (20 µM)			9.66				

Table 2. Effect of naringenin derivatives (**32**-**39**) on P-gp mediated R123 efflux, in *ABCB1*-transfected mouse T-lymphoma (L5178Y-MDR) cells.

			Fluorescence Activity Ratio (FAR)	
Compound	**log*P*** [a]	**pKa amine** [b]	**2.0 µM**	**20 µM**
32	2.97	--	1.17	1.83
33	3.16	--	1.33	13.30
34	3.23	9.36	4.06	36.25
35	3.37	9.06	3.08	30.76
36	2.73	7.83	8.01	43.68
37	3.88	7.01; 9.67	18.70	62.09
38	4.61	16.82	0.86	6.65
39	4.67	---	0.92	12.78
DMSO (2%)			1.01	
Verapamil (20 µM)			9.66	

[a] calculated in MarvinSketch v17.24.0; [b] compound **37** has two protonated nitrogen atoms.

Table 4. Interaction type between compounds **23**, **31** and **37** with doxorubicin on L5178Y-MDR cells.

Compound	**Ratio** [a]	**CI ± SD** [b]	**Interaction**
23	6:1	0.638 ± 0.248	Synergism
31	8:1	0.445 ± 0.190	Synergism

[a] Data are shown as the best combination ratio between compounds and doxorubicin. [b] Combination index (CI) values are represented as the mean of three CI values calculated from different drug ratios ± standard deviation (SD) of the mean, for an inhibitory concentration of 50% (IC_{50}). CI < 0.1, very strong synergism; 0.1 < CI < 0.3, strong synergism; 0.3 < CI < 0.7, synergism; 0.7 < CI < 0.9, moderate to slight synergism; 0.9 < CI < 1.1, additivity.

2.5. Flavanone Derivatives as Competitive Modulators

The analysis of the flavanone-protein interactions was initially performed by molecular docking studies, using a previously refined murine P-gp structure.[14,15] A potential alternate binding site involving residues Glu502 and Phe792 (Glu522 and Phe800 in murine P-gp, respectively), identified in an *A. thaliana* P-gp homologue,[16] guided the initial definition of the docking sites. Following, from binding studies with photo-reactive dihydropyridine derivatives[17,18] and flavonoids[19] other amino acids were used to define the docking box, namely amino acids 230-312 and 468-527.

When docked at the internal drug-binding pocket (*Supporting information*, Table S3), 92% (36/39) had their top-ranked docking pose at a previously assigned R-site,[14] with only three compounds (**12**, **15** and **37**) assigned to the modulator M-site (*Supporting information*, Table S3). Therefore, the docking results suggest that most of the flavanone derivatives exert their activity by competing with R123 for the substrate-binding site, therefore classified as competitive efflux modulators. Concerning the docking results at the nucleotide-binding domains, seven were found at the NBD1 and nine at the NBD2 having a $\Delta\Delta G_{bind}$ < 1.0 kcal.mol^{-1} with the docking scores inside the transmembrane drug-binding cavity. Herein, it is worth noticing that i) compound **13** (a thiosemicarbazone) was the only one with more favorable binding energies at NBD2 and ii) compounds **32**-**36** also revealed favorable interactions with NBD1. As both locations were experimentally involved in P-gp folding, trafficking and activity,[20–22] we hypothesize that an alternative mechanism of action may derive from specific interactions within these regions. Thus, and apart from a competitive modulation mechanism, the herein reported flavanone hydrazones may also act as allosteric efflux modulators when bound at these specific domains.

2.6. In Silico Evaluation of Hydroxyl Methylation in Membrane Permeation

The effect that methylation of the phenolic hydroxyls on the MDR reversal activity is of particular interest. Thus, for the series comprising non-, *O*-mono- and *O*-dimethylated compounds with identical C-4 substituents, a comparison of the obtained FAR values was performed and as depicted in Figure 2. While at 2.0 µM the methylation of both C-7 and C-4' hydroxyls maintained or improved the MDR-reversal activity of most of the compounds, at 20 µM the best results were obtained for the monomethylated derivatives excepting for compound **29** (Table 2).

One possible explanation for the effect of methylation on the activity is related with the ability of methylated flavonoids to permeate much faster into the lipid membrane.[23,24] Thus, and for the compounds series with the most distinct MDR-reversal activities (**4**, **17**, **27** and **12**, **23**, **31**), by using the PerMM online server [25,26] for passive membrane permeation it was verified that, methylation lowers the energetic barrier for

cros the
However, while the obtained results suggest that decreasing the energetic penalty associated with leaflet "flip-flop", they only partially explain the observed activities.

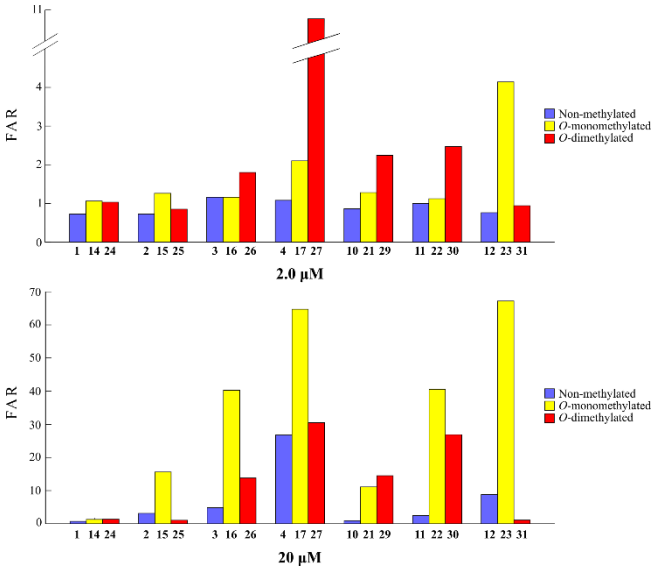

Figure 2. Effect of the methylation on phenolic hydroxyls on R123 accumulation in L5178Y-MDR cells, at both 2.0 µM and 20 µM.

2.7. Evaluation of Protein-Ligand Interactions

To gain additional insights on how the methylation is expected to influence the interaction of the molecules with P-gp, we proceeded through molecular dynamics (MD) simulations. In the field of natural products, Molecular Dynamics (MD) techniques are increasingly being used to better understand how molecules specifically interact with a given target.[27,28] Herein, and concerning hydrazone derivatives **4**, **17** and **27**, the relative binding affinity increases with methylation. Oppositely, for the series of compounds **12**, **23** and **31** the derivative with the highest activity, **23** (FAR = 4.14 and 67.24, at 2 and 20 µM, respectively) was estimated to have a higher relative ΔG_{bind} (-39.6 ± 3.4 kcal.mol^{-1}) (Table 5). As ligand efficiency (LE, see Material and Methods) also increased with methylation in the former (**4**, LE = 0.27; **17**, LE = 0.41; **27**, LE = 0.37) but not in the latter (**12**, LE = 0.26; **23**, LE = 0.28; **31**, LE = 0.25), the initial perusal of MD data suggests that methylation have a greater contribution for the binding of hydrazone derivatives. This was also corroborated by the decrease in the ability of compounds **17** and **27** to form hydrogen bonds (HB) when compared with **4**. In the other series, only in **23** a weakening of the protein-ligand HB network could be inferred (Table 5).

Visual evaluation of the MD simulations revealed that both mono- and dimethylated hydrazones **17** and **27** shifted from their original position within the binding pocket, with compound **27** reaching the lower limit of a previously reported modulator M-site (Figure S63).[15,29] We performed an additional MD simulation with compound 27 at the M-site and registered a decrease in its ΔG_{bind}, to -60.4 ± 3.4 kcal.mol^{-1} and a substantial increase in its cross interaction capability (CIc = 90%, see Material and Methods).[13] Therefore, and concerning the hydrazone derivatives, *O*-methylation seems to decrease the affinity towards the substrate-binding R and H sites, while favoring binding to the modulator M-site.[15,30,31]

Compounds **12**, **23** and **31**, however, are always found bound to the drug-binding R site, a site found to be involved in R123 transport.[32] Interestingly, compound **23** was found to R site, mainly due to intramolecular CH-π interactions between the NH group and the phenyl ring of the substituent. This interaction was also found to re-orientate the hydrazide moiety in a way that it becomes unable to establish HBs with the surrounding residues (*Supporting Information*, Figure S63). Therefore, the data suggest that, in this set of naringenin derivatives, the higher activity observed for the monomethylated compound is due to the distinct conformation that **23** adopt while in the R site. Hypothetically, the decrease in the binding affinity of compound **23** does not prevent it from being effluxed and, if achieving higher turnover rates than the fluorescent dye,[33,34] an effect similar to R123 efflux inhibition can be expected.

Molecular docking also suggested that some derivatives may bind to the TMD/NBD interfaces (*Supporting Information*, Table S3). After performing two additional MD simulations with compounds **13** and **32** at the NBD2 and NBD1, respectively, such results were corroborated by the negative ΔG_{bind} obtained (**13**: -14.8 ± 4.4 kcal.mol^{-1}; **32**: -18.2 ± 8.4 kcal.mol^{-1}). However, higher ligand efficiency and hydrogen bonding were estimated for **13** (LE = 0.16; $\langle N_{HB} \rangle$, 1.395; τ, 2478 ps; ΔG_{HB}, -24.9 kJ.mol^{-1}) when compared with **32** (LE = 0.08; $\langle N_{HB} \rangle$, 0.621; τ, 1256 ps; ΔG_{HB}, -23.2 kJ.mol^{-1}). Nevertheless, both molecules interacted with residues involved in the activation/inhibition of P-gp ATPase activity (Trp158/Phe159/Phe900, equivalent to Trp162, Phe163 and Phe904 in human P-gp)[20,35] at the NBD1, or in P-gp maturation (Ile257/Arg258, corresponding to Ile261 and Arg262 in human P-gp) at NBD2.[21,22] Therefore, these results are in agreement with previous experimental data and do not exclude the possibility that naringenin derivatives may act as allosteric efflux modulators, when interacting in these particular regions.

Table 5. Data from MD Simulations for Compounds **4**/**17**/**27** and 12/23/31 series.

	4	17	27	12	23	31
Molecular Mechanics/Poisson-Boltzmann Surface Area (MM/PBSA) binding energies [a]						
ΔG_{bind} ± SD (kcal.mol^{-1})	-38.6 ± 3.9	-49.8 ± 4.3	-55.6 ± 2.9	-46.6 ± 4.1	-39.6 ± 3.4	-45.7 ± 3.4
Protein-Ligand Interactions						
LE	0.27	0.41	0.37	0.26	0.28	0.25
Hydrogen bonding [b]						
$\langle N_{HB} \rangle$	1.359	1.578	1.336	1.887	1.116	1.877
ΔG_{HB} (kcal.mol^{-1})	-5.5	-5.2	-4.8	-5.4	-5.2	-5.8
τ (ps)	1167	743	383	1023	702	1837

[a] ΔG_{bind}, relative free-energy of binding; [b] ΔG_{HB}, hydrogen-bond formation energy; $\langle N_{HB} \rangle$, average number of hydrogen-bonds per time frame; τ, hydrogen bond lifetime.

3. Conclusion

Summarizing, following our previous work on developing novel flavonoid derivatives as MDR-reversal agents, the chemical modification of the flavanone scaffold was further pursued by expanding the available pool of flavanone-based MDR reversal agents. When compared with the previously set of derivatives without methoxy groups, both *O*-monomethylation and *O*-dimethylation were found to improve P-gp modulation. More importantly, the results showed that the MDR reversal activity of the flavanone scaffold improves by adding nitrogen atoms and aromatic moieties to either C-4 or C-4', with the activities of the latter apparently increasing with

the [illegible] n, 3 constant of the positively charged nitrogen (**34-38**). Finally, in chemosensitivity experiments, drug combination assays of selected compounds with the anticancer drug doxorubicin corroborated the anti-MDR potential of these derivatives due to synergistic interaction.

While from molecular docking was inferred that most of the derivatives act as competitive inhibitors at the substrate-binding R and H sites, further *in silico* studies provided additional insights on the role of methylation for the observed biological activity. Permeation studies using the PerMM server clarified that both mono- and dimethylation decreases the energetic barrier for membrane permeation. Molecular Dynamics simulations showed that, while in hydrazones (**4**, **17** and **27**) dimethylation increases the binding affinity towards the modulator M-site, carbohydrazides (**12**, **23** and **31**) revealed small or no changes in the binding affinities towards R site. Instead, more folded conformations when at this drug-binding site were observed, especially for the monomethylated derivative, leading us to hypothesize that **23** can act as a high-turnover substrate. Finally, when bound to the TMD/NBD interfaces, MD simulations also clarified that the flavanone scaffold may be a suitable building block for developing novel allosteric efflux modulators, thus overcoming many of the problems identified in the early generations of efflux inhibitors. Further studies are currently ongoing to clarify the potential of these compounds to act as allosteric efflux inhibitors.

4. Experimental Procedures

4.1. General chemistry

All reagents were obtained from commercial suppliers and used without further purification while solvents were used after distillation. Mass spectra were obtained by LC-MS on a Triple Quadrupole mass spectrometer (Micromass Quattro Micro API, Waters, Milford, MA, USA). Column and preparative thin-layer chromatography were performed with silica gel 60 (0.040–0.063 mm, Merck, Darmstadt, Germany) and GF_{254} (Merck, Darmstadt, Germany), respectively. All reactions were monitored by thin-layer chromatography (TLC) by using TLC silica 60 F_{254}-coated aluminum plates, visualized under UV light and by spraying them with sulfuric acid/methanol (1:1) and heated. NMR spectra were recorded on a Brüker 300 Ultra-Shield (^{1}H 300 MHz; ^{13}C 75 MHz). ^{1}H and ^{13}C chemical shifts are expressed in δ (ppm) referenced to the solvent used and the proton coupling constants J in Hz. Spectra were assigned using appropriate COSY, DEPT, HMQC and HMBC sequences. The purity of all compounds (≥ 95%) was determined on a HPLC-UV system (Merck-Hitachi) using a Merck LiChrospher 100 RP-18 column (5 µm, 125 × 4 mm) and MeOH/H_2O mixtures as mobile phases. The preparation of the non-methylated compounds **2-13** was performed as previously described.[7]

4.1.1. O-Methylation of naringenin (1) with dimethyl sulfate.

To compound 1 (1.0 g, 1 equiv.) in a proper amount of acetone were added dimethyl sulfate (1.1 equiv.) and potassium carbonate (K_2CO_3, 3 equiv.) while the mixture was kept in reflux (50 °C) overnight under constant stirring.[28] The reaction was followed by TLC and, upon completion, the solvent was evaporated under vacuum at 40 °C, the residue extracted with ethyl acetate and dried with Na_2SO_4. After evaporation of the solvent, the residue was further purified by column chromatography (CH_2Cl_2:acetone, 1:0 to 4:1) to obtain equiv. of dimethyl sulphate were used.

Sakuranetin, (*S,E*)-5-hydroxy-2-(4-hydroxyphenyl)-7-methoxy-2,3-dihydrochromen-4-one (**14**). Amorphous orange power (799 mg, yield 76%). ^{1}H NMR (300 MHz, Acetone-D6) δ = 7.40 (d, J = 8.4 Hz, 2 H), 6.90 (d, J = 8.4 Hz, 2 H), 6.04 (m, 2H), 5.48 (dd, J = 12.9, 3.0 Hz, 1 H), 3.85 (s, 3 H), 3.22 (dd, J = 17.2, 12.9 Hz, 1 H), 2.75 (dd, J = 17.2, 3.0 Hz, 1 H); ^{13}C NMR (75 MHz, Acetone-D6) δ = 197.6, 168.8, 166.9, 164.9, 158.8, 130.5, 129.0, 116.1, 103.8, 95.4, 94.5, 80.0, 56.2, 43.4. LRMS (ESI) *m/z* (positive mode) 287 $[M + H]^+$.

4'-methoxysakuranetin, (*S,E*)-5-hydroxy-2-(4-methoxyphenyl)-7-methoxy-2,3-dihydro chromen-4-one (**24**). Amorphous orange power (176 mg, yield 16%). ^{1}H NMR (300 MHz, Acetone-D6) δ = 7.49 (d, J = 8.6 Hz, 2 H), 7.00 (d, J = 8.6 Hz, 2 H), 6.05 (m, 2 H), 5.53 (dd, J = 12.8, 3.0 Hz, 2 H), 3.86 (s, 3 H), 3.83 (s, 3 H), 3.22 (dd, J = 17.2, 12.8 Hz, 1 H), 2.78 (dd, J = 17.1, 3.0 Hz, 1 H); ^{13}C NMR (75 MHz, Acetone-D6) δ = 197.5, 168.8, 165.0, 164.1, 160.9, 131.8, 128.9, 114.8, 103.7, 95.5, 94.6, 79.8, 56.2, 55.6, 43.5. LRMS (ESI) *m/z* (positive mode) 301 $[M + H]^+$.

4.1.2. General preparation of hydrazone derivatives 15 and 25.

Each starting compound (**14** or **24**, 400 mg, 1 equiv.) was dissolved in a solution of hydrazine monohydrate (2 mL, 63.7 mmol) and was kept stirring 24 h at 50 ºC, under nitrogen. The mixture was evaporated, and the residue was purified by column chromatography (*n*-hexane:EtOAc, 1:0 to 0:1) to afford the desired compound.

(*S,E*)-5-hydroxy-2-(4-hydroxyphenyl)-7-methoxy-2,3-dihydrochromen-4-hydrazone (**15**). Amorphous orange power (285 mg, yield 68 %). ^{1}H NMR (300 MHz, DMSO-D6) δ = 7.30 (d, J = 8.4 Hz, 2 H), 6.78 (d, J = 8.5 Hz, 2 H), 6.07 (d, J = 2.2 Hz, 1 H), 6.05 (d, J = 2.2 Hz, 1 H), 5.15 (dd, J = 12.0, 2.6 Hz, 1 H), 3.73 (s, 3 H), 3.53 (dd, J = 17.2, 2.8 Hz, 1 H), 2.94 (dd, J = 17.2, 12.2 Hz, 1 H); ^{13}C NMR (75 MHz, DMSO-D6) δ = 163.6, 162.2, 161.8, 159.8, 157.6, 129.6, 128.2, 115.2, 99.3, 95.1, 93.6, 76.6, 55.4, 31.6 ppm. LRMS (ESI) *m/z* (positive mode) 342 $[M + H + ACN]^+$.

(*S,E*)-5-hydroxy-2-(4-methoxyphenyl)-7-methoxy-2,3-dihydrochromen-4-hydrazone (**25**). Amorphous brownish powder (355 mg, yield 85 %). ^{1}H NMR (300 MHz, DMSO-D6) δ = 7.43 (d, J = 8.7 Hz, 2 H), 6.96 (d, J = 8.7 Hz, 2 H), 6.07 (q, J = 2.4 Hz, 2 H), 5.23 (dd, J = 11.9, 3.0 Hz, 1 H), 3.76 (s, 3 H), 3.73 (s, 3 H), 3.54 (dd, J = 17.3, 3.0 Hz, 1 H), 2.99 (dd, J = 17.3, 11.9 Hz, 1 H); ^{13}C NMR (75 MHz, DMSO-D6) δ 164.0, 162.2, 162.0, 160.1, 159.7, 131.4, 128.2, 113.9, 99.4, 95.1, 93.6, 76.0, 55.5, 55.2, 31.7 ppm. LRMS (ESI) *m/z* (positive mode) 355 $[M + H + ACN]^+$.

4.1.3. General procedure for the preparation of O-methylated hydrazones.

To 1 equiv. of compound **14** or **24** dissolved in ethanol was added 2 equiv. of the desired hydrazine (NH_2-NH-R) and 0.01 equiv. of 10% acetic acid in ethanol. Following, the mixture was stirred under nitrogen, at room temperature, until the total disappearance of the starting compound (by TLC). Then, the solvent was evaporated, the residue extracted with ethyl acetate, dried (with Na_2SO_4) and further purified by preparative TLC to obtain the corresponding hydrazone (C=N-NH-R).

(*S,E*)-5-hydroxy-2-(4-hydroxyphenyl)-7-methoxy-2,3-dihydrochromen-4-phenylhydrazone (**16**). Amorphous yellow powder, obtained by reacting 20 mg of compound **14** with

phen
Acetone-D6) δ = 7.37 (d, J = 8.6 Hz, 2 H), 7.24 (dd, J = 8.6, 7.4 Hz, 2 H), 7.03 (dd, J = 8.6, 1.0 Hz, 2 H), 6.88 (d, J = 8.6 Hz, 2 H), 6.81 (td, J = 7.4, 1.0 Hz, 1 H), 6.08 (d, J = 2.5 Hz, 1 H), 6.01 (d, J = 2.5 Hz, 1 H), 5.08 (dd, J = 12.1, 3.2 Hz, 1 H), 3.73 (s, 3 H), 3.26 (dd, J = 16.8, 3.2 Hz, 1 H), 2.77 (dd, J = 16.8, 12.1 Hz, 1 H); ^{13}C NMR (75 MHz, Acetone-D6) δ = 162.8, 160.7, 159.1, 158.5, 146.1, 145.6, 132.0, 130.1, 128.8, 120.7, 116.1, 113.3, 101.0, 96.2, 94.5, 77.4, 55.6, 32.6 ppm. LRMS (ESI) *m/z* (positive mode) 377 $[M + H]^+$.

(*S,E*)-5-hydroxy-2-(4-hydroxyphenyl)-7-methoxy-2,3-dihydrochromen-4-(5-bromopyridin-2-yl)hydrazone (**17**). Amorphous brown powder, isolated after the reaction of compound **14** with 5-bromopyridin-2-yl-hydrazine (12 mg, 37% yield). ^{1}H NMR (300 MHz, Acetone-D6) δ = 8.24 (d, J = 2.4 Hz, 1 H), 7.82 (dd, J = 8.5, 2.4 Hz, 1 H), 7.45 (d, J = 8.5 Hz, 1 H), 7.41 (d, J = 8.6 Hz, 2 H), 6.91 (d, J = 8.6 Hz, 2 H) 6.11 (d, J = 2.5 Hz, 1 H), 6.06 (d, J = 2.5 Hz, 1 H), 5.08 (dd, J = 11.9, 3.4 Hz, 1 H), 3.73 (s, 3 H), 3.40 (dd, J = 16.5, 3.4 Hz, 1 H), 2.94 (dd, J = 16.5, 11.9 Hz, 1 H); ^{13}C NMR (75 MHz, Acetone-D6) δ = 163.3, 161.2, 160.6, 159.6, 155.4, 149.6, 145.6, 141.2, 131.7, 128.8, 116.1, 116.0, 110.5, 100.4, 96.4, 94.5, 77.4, 55.7, 32.6 ppm. LRMS (ESI) *m/z* (positive mode) 497 $[M + H + ACN]^+$.

(*S,E*)-5-hydroxy-2-(4-methoxyphenyl)-7-methoxy-2,3-dihydrochromen-4-phenylhydrazone (**26**): obtained as an amorphous brown powder by the reaction of compound **24** (20 mg) with phenylhydrazine (9 mg, 34% yield). ^{1}H NMR (300 MHz, Acetone-D6) δ = 7.50 (d, J = 8.6 Hz, 2 H), 7.28 (dd, J = 8.6, 7.4 Hz, 2 H), 7.06 (dd, J = 8.6, 1.1 Hz, 2 H), 7.01 (d, J = 8.6 Hz, 2 H), 6.85 (td, J = 7.4, 1.1 Hz, 1 H), 6.12 (d, J = 2.5 Hz, 1 H), 6.06 (d, J = 2.4 Hz, 1 H), 5.17 (dd, J = 12.0, 3.1 Hz, 1 H), 3.83 (s, 3 H), 3.78 (s, 3 H), 3.32 (dd, J = 16.8, 3.1 Hz, 1 H), 2.79 (dd, J = 16.8, 12.0 Hz, 1 H); ^{13}C NMR (75 MHz, Acetone-D6) δ = 62.8, 160.8, 160.7, 159.0, 146.1, 145.6, 133.1, 130.1, 128.7, 120.7, 114.7, 113.3, 101.1, 96.3, 94.5, 77.2, 55.7, 55.6, 32.5 ppm. LRMS (ESI) *m/z* (positive mode) 391 $[M + H]^+$.

(*S,E*)-5-hydroxy-2-(4-methoxyphenyl)-7-methoxy-2,3-dihydrochromen-4-(5-bromopyridin-2-yl)hydrazone (**27**). Amorphous yellow powder, from the reaction of compound **24** with 5-bromopyridin-2-yl-hydrazine (8 mg, 37% yield). ^{1}H NMR (300 MHz, Acetone-D6) δ = 8.24 (d, J = 2.4 Hz, 1 H), 7.82 (dd, J = 8.8, 2.4 Hz, 1 H), 7.51 (d, J = 8.8 Hz, 2 H), 7.01 (d, J = 8.7 Hz, 2 H), 6.93 (d, J = 8.7 Hz, 2 H), 6.12 (d, J = 2.5 Hz, 1 H), 6.07 (d, J = 2.5 Hz, 1 H), 5.20 (dd, J = 12.5, 2.9 Hz, 1 H), 3.83 (d, J = 0.9 Hz, 3H), 3.78 ppm (s, 3 H), 3.43 (dd, J = 16.6, 2.9 Hz, 1 H), 2.96 (dd, J = 16.6, 12.5 Hz, 1 H); ^{13}C NMR (75 MHz, Acetone-D6) δ = 163.5, 162.8, 161.3, 160.9, 156.6, 149.6, 148.9, 141.6, 132.8, 128.8, 114.7, 109.2, 109.0, 100.9, 95.5, 94.6, 77.2, 55.7, 55.6, 32.5 ppm. LRMS (ESI) *m/z* (positive mode) 470 $[M + H]^+$.

4.1.4. General procedure for the preparation of carbohydrazides.

To 20 mg of compounds **14** or **24** (1.0 equiv.) dissolved in a proper amount of ethanol was added the desired hydrazide (2 equiv.), a catalytic amount of acid (10% acetic acid in ethanol, 0.01 eq) and the mixture was kept stirring under nitrogen overnight, at room temperature. The reaction was followed by TLC and, upon completion, the solvent was evaporated under vacuum at 40 ºC, the residue extracted with ethyl acetate and dried with Na_2SO_4. After evaporation of the solvent, the residue was further purified by preparative TLC to obtain the desired product (R^1=N-NH-CO-R^2).

dihydrochromen-4-(p-trifluormethylphenyl)-carbohydrazide (**18**). Amorphous orange brownish powder, obtained from the reaction of compound **14** with 4-trifluormethylphenyl-hydrazide. (12 mg, 33% yield). ^{1}H NMR (300 MHz, Acetone-D_6) δ = 8.07 (d, J = 8.0 Hz, 1H), 7.87 (d, J = 8.0 Hz, 1H), 7.34 (d, J = 8.2 Hz, 2H), 6.81 (d, J = 8.2 Hz, 2H), 6.11 (d, J = 2.3 Hz, 1H), 6.06 (d, J = 2.3 Hz, 1H), 5.14 (br d, J = 13.0 Hz, 1H), 3.74 (s, 3H), 3.43 (br d, J = 16.3 Hz, 1H), 2.99 (dd, J = 16.3, 13.0 Hz, 1H) ppm; ^{13}C NMR (75 MHz, acetone-D_6) δ 167.0, 163.1, 161.0, 159.3, 157.7, 155.0, 137.6, 132.1, 129.6, 129.1, 128.3, 125.4, 115.2, 99.3, 95.5, 93.7, 76.4, 55.4, 32.3 ppm; ESIMS *m/z* (positive mode) 473 $[M + H]^+$.

(*S,E*)-5-hydroxy-2-(4-hydroxyphenyl)-7-methoxy-2,3-dihydrochromen-4-(tiophen-2-yl)-hydrazide (**19**). Amorphous orange brownish powder, synthesized from the reaction of compound **14** with 2-thiophene-carboxyhydrazide (6 mg, 21% yield). ^{1}H NMR (300 MHz, Acetone-D6) δ = 7.87 (br s, 1 H), 7.78 (d, J = 4.9 Hz, 1 H), 7.41 (d, J = 8.4 Hz, 2 H), 7.14 (br d, J = 4.9 Hz, 1 H), 6.91 (d, J = 8.4 Hz, 2 H), 6.11 (d, J = 2.5 Hz, 1 H), 6.04 (d, J = 2.5 Hz, 1 H), 5.16 (dd, J = 12.0, 1.9 Hz, 1 H), 3.79 (s, 3 H), 3.44 (dd, J = 16.5, 1.9 Hz, 1 H), 2.96 (dd, J = 16.5, 12.0 Hz, 1 H); ^{13}C NMR (75 MHz, Acetone-D6) δ = 164.8, 162.4, 160.6, 158.6, 156.6, 148.5, 140.6, 132.4, 131.5, 128.9, 128.6, 126.6, 116.1, 100.9, 96.4, 95.9, 78.5, 55.8, 32.9 ppm. LRMS (ESI) *m/z* (positive mode) 411 $[M + H]^+$.

(*S,E*)-5-hydroxy-2-(4-hydroxyphenyl)-7-methoxy-2,3-dihydrochromen-4-(p-aminophenyl)-hydrazide (**20**). Obtained as an amorphous orange brownish powder from the reaction of compound **14** with 4-aminophenyl-carboxyhydrazide (6 mg, 20% yield). ^{1}H NMR (300 MHz, Acetone-D6) δ = 7.72 (d, J = 8.1 Hz, 2 H), 7.40 (d, J = 7.9 Hz, 2 H), 6.90 (d, J = 8.0 Hz, 2 H), 6.67 (d, J = 7.9 Hz, 2 H), 6.10 (d, J = 2.4 Hz, 1 H), 6.04 (d, J = 2.4 Hz, 1 H), 5.14 (br d, J = 11.5 Hz, 1 H), 3.78 (s, 3 H), 3.44 (br d, J = 16.4 Hz, 1 H), 3.01 (dd, J = 16.4, 11.5 Hz, 1 H); ^{13}C NMR (75 MHz, Acetone-D6) δ = 164.8, 163.9, 162.2, 160.2, 158.6, 157.7, 153.2, 131.6, 130.4, 128.9, 121.2, 116.1, 113.9, 100.6, 96.3, 94.3, 77.6, 55.7, 32.8 ppm. LRMS (ESI) *m/z* (positive mode) 420 $[M + H]^+$.

(*S,E*)-5-hydroxy-2-(4-hydroxyphenyl)-7-methoxy-2,3-dihydrochromen-4-(furan-2-yl)-hydrazide (**21**). Amorphous orange brownish powder, obtained from the reaction of compound **14** with 2-furan carboxylic acid hydrazide (11 mg, 41% yield). ^{1}H NMR (300 MHz, Acetone-D6) δ = 7.72 (d, J = 1.6 Hz, 1 H), 7.40 (d, J = 7.8 Hz, 2 H), 7.24 (br s, 1 H), 6.91 (d, J = 7.8 Hz, 2 H), 6.63 (br s, 1 H), 6.10 (d, J = 2.4 Hz, 1 H), 6.04 (d, J = 2.4 Hz, 1 H), 5.16 (br d, J = 13.5 Hz, 1 H), 3.79 (s, 3 H), 3.43 (br d, J = 16.0 Hz, 1 H), 3.00 (dd, J = 16.0, 13.5 Hz, 1 H); ^{13}C NMR (75 MHz, Acetone-D6) δ = 164.4, 163.6, 162.3, 158.6, 155.0, 147.8, 147.2, 145.6, 131.4, 128.9, 116.1, 116.0, 112.9, 100.4, 96.4, 94.5, 77.6, 55.7, 32.9 ppm. LRMS (ESI) *m/z* (positive mode) 395 $[M + H]^+$.

(*S,E*)-5-hydroxy-2-(4-hydroxyphenyl)-7-methoxy-2,3-dihydrochromen-4-(1H-indol-3-yl)-acetohydrazide (**22**). Amorphous yellow powder, from the reaction of compound **14** with 3-indoleacetic acid hydrazide (12.3 mg, 38% yield). ^{1}H NMR (300 MHz, Acetone-D6) δ = 7.64 (d, J = 7.5 Hz, 1 H), 7.37 (d, J = 8.0 Hz, 2 H), 7.33 (d, J = 7.5 Hz, 1 H), 7.30 (s, 1 H), 7.08 (t, J = 7.5 Hz, 1 H), 6.99 (t, J = 7.5 Hz, 1 H), 6.89 (d, J = 8.0 Hz, 2 H), 6.06 (d, J = 2.5 Hz, 1 H), 6.00 (d, J = 2.5 Hz, 1 H), 5.08 (br d, J = 13.6 Hz, 1 H), 3.80 (s, 2 H), 3.76 (s, 3 H), 3.15 (br d, J = 16.0 Hz, 1 H), 2.75 (dd, J = 16.0, 13.6 Hz, 1 H); ^{13}C NMR (75 MHz, Acetone-D6) δ = 167.7, 164.0, 162.1, 160.2, 158.6, 152.4, 137.5, 131.4, 128.8, 128.4, 124.7, 122.2, 119.7,

119. 7.1, 32.2 ppm. LRMS (ESI) *m/z* (positive mode) 458 [*M* + H]$^+$.

(*S,E*)-5-hydroxy-2-(4-hydroxyphenyl)-7-methoxy-2,3-dihydrochromen-4-(1-phenoxyformo)-hydrazide (**23**). Amorphous orange brownish powder, isolated after the reaction of compound **14** with benzyl carbazate (29 mg, 92% yield). ^{1}H NMR (300 MHz, Acetone-D6) δ = 7.52-7.26 (m, 7 H), 6.90 (d, *J* = 8.4 Hz, 2 H), 6.09 (d, *J* = 2.5 Hz, 1 H), 6.04 (d, *J* = 2.4 Hz, 1 H), 5.23 (s, 2 H), 5.13 (dd, *J* = 12.0, 2.6 Hz, 1 H), 3.78 (s, 3 H), 3.32 (dd, *J* = 16.7, 2.6 Hz, 1 H), 2.86 (dd, *J* = 16.7, 12.0 Hz, 1 H); ^{13}C NMR (75 MHz, Acetone-D6) δ = 163.7, 161.7, 160.0, 158.5, 151.8, 137.5, 131.5, 129.3, 129.0, 128.7, 116.1, 100.4, 96.3, 94.4, 77.2, 67.6, 55.7, 32.5 ppm. LRMS (ESI) *m/z* (positive mode) 435 [*M* + H]$^+$.

(*S,E*)-5-hydroxy-2-(4-methoxyphenyl)-7-methoxy-2,3-dihydrochromen-4-(p-aminophenyl)-hydrazide (**28**). Amorphous orange brownish powder, obtained by reacting compound **24** with 4-aminophenyl-carboxyhydrazide (8 mg, 27% yield). ^{1}H NMR (300 MHz, DMSO-D6) δ = 7.64 (d, *J* = 8.5 Hz, 2 H), 7.46 (d, *J* = 8.5 Hz, 2 H), 7.00 (d, *J* = 8.5 Hz, 2 H), 6.57 (d, *J* = 8.5 Hz, 2 H), 6.09 (d, *J* = 2.4 Hz, 1 H), 6.04 (d, *J* = 2.4 Hz, 1 H), 5.18 (dd, *J* = 12.2, 2.2 Hz, 1 H), 3.78 (s, 3 H), 3.73 (s, 3 H), 3.48 (dd, *J* = 17.0, 2.2 Hz, 1 H), 2.97 (dd, *J* = 17.0, 12.2 Hz, 1 H); ^{13}C NMR (75 MHz, DMSO-D6) δ = 164.5, 162.4, 160.6, 159.4, 158.7, 152.5, 152.1, 131.5, 129.8, 128.1, 118.9, 113.0, 112.5, 99.6, 95.4, 93.5, 76.0, 55.3, 55.2, 32.0 ppm. LRMS (ESI) *m/z* (positive mode) 434 [*M* + H]$^+$.

(*S,E*)-5-hydroxy-2-(4-methoxyphenyl)-7-methoxy-2,3-dihydrochromen-4-(furan-2-yl)-hydrazide (**29**). Amorphous orange brownish powder, obtained by reacting compound **24** with 2-furan carboxylic acid hydrazide (13 mg, 45% yield). ^{1}H NMR (300 MHz, Acetone-D6) δ = 7.72 (d, *J* = 1.7 Hz, 1 H), 7.50 (d, *J* = 8.6 Hz, 2 H), 7.23 (d, *J* = 3.5 Hz, 1 H), 7.01 (d, *J* = 8.6 Hz, 2 H), 6.63 (dd, *J* = 2.8, 1.4 Hz, 1 H), 6.11 (d, *J* = 2.5 Hz, 1 H), 6.05 (d, *J* = 2.5 Hz, 1 H), 5.20 (dd, *J* = 12.4, 1.4 Hz, 1 H), 3.83 (s, 3 H), 3.79 (s, 3 H), 3.45 (dd, *J* = 16.5, 1.4 Hz, 1 H), 3.01 (dd, *J* = 16.5, 12.4 Hz, 1 H); ^{13}C NMR (75 MHz, Acetone-D6) δ = 164.4, 162.3, 160.8, 160.3, 155.1, 147.8, 146.8, 145.6, 132.6, 128.7, 116.1, 114.7, 112.9, 100.4, 96.4, 94.5, 77.4, 55.8, 55.6, 32.9 ppm. LRMS (ESI) *m/z* (positive mode) 409 [*M* + H]$^+$.

(*S,E*)-5-hydroxy-2-(4-methoxyphenyl)-7-methoxy-2,3-dihydrochromen-4-(1H-indol-3-yl)-acetohydrazide (**30**). Amorphous yellow powder, from the reaction of compound **24** with 3-indoleacetic acid hydrazide (11.1 mg, 34% yield). ^{1}H NMR (300 MHz, DMSO-D6) δ = 7.58 (br d, *J* = 7.8 Hz, 1 H), 7.47 (d, *J* = 8.5 Hz, 2 H), 7.34 (d, *J* = 7.8 Hz, 1 H), 7.23 (br s, 1 H), 7.06 (br t, *J* = 7.8 Hz, 1 H), 7.00 (d, *J* = 8.5 Hz, 1 H), 6.95 (br t, *J* = 7.8 Hz, 1 H), 6.50 (d, *J* = 2.2 Hz, 1 H), 6.03 (d, *J* = 2.2 Hz, 1 H), 5.20 (br d, *J* = 12.5 Hz, 1 H), 3.78 (s, 3 H), 3.72 (s, 2 H), 3.71 (s, 3 H), 3.31 (br d, *J* = 16.9 Hz, 1 H), 2.95 (dd, *J* = 16.9, 12.5 Hz, 1 H); ^{13}C NMR (75 MHz, DMSO-D6) δ = 167.5, 167.4, 162.5, 159.4, 158.7, 150.8, 136.1, 131.4, 128.1, 127.2, 123.9, 121.0, 118.7, 118.4, 113.9, 111.4, 108.3, 99.3, 95.4, 93.6, 75.8, 55.3, 55.2, 32.7, 30.7 ppm. LRMS (ESI) *m/z* (positive mode) 472 [*M* + H]$^+$.

(*S,E*)-5-hydroxy-2-(4-methoxyphenyl)-7-methoxy-2,3-dihydrochromen-4-(1-phenoxyformo)-hydrazide (**31**). Amorphous orange brownish powder, from the reaction of compound **24** with benzyl carbazate (14.9 mg, 47% yield). ^{1}H NMR (300 MHz, DMSO-D6) δ = 7.45-7.32 (m, 7 H), 6.98 (d, *J* = 8.7 Hz, 2 H), 6.07 (d, *J* = 2.4 Hz, 1 H), 6.05 (d, *J* = 2.4 Hz, 1 H), 5.21 (s, 2 H), 5.17 (dd, *J* = 12.0, 2.8 Hz, 1 H), 3.77 (s, 3 H), 12.0 Hz, 1 H); ^{13}C NMR (75 MHz, DMSO-D6) δ = 162.2, 162.2, 160.0, 159.3, 158.3, 152.2, 144.4, 131.6, 128.5, 128.4, 127.9, 113.8, 99.4, 95.4, 93.6, 75.8, 66.4, 55.3, 55.1, 34.0 ppm. LRMS (ESI) *m/z* (positive mode) 449 [*M* + H]$^+$.

4.1.5. Reaction of sakuranetin with epichlorohydrin.

To 200 mg (1 equiv.) of compound **14** dissolved in ethanol was added 1.5 equiv. of epichlorohydrin. Following, 1.1 equiv. of NaOH (dissolved in ethanol) was added to the mixture and the reaction was refluxed overnight followed by evaporation to dryness under reduced pressure. The residue was then dissolved in ethyl acetate and washed twice with water. The organic layer was dried over Na_2SO_4 and after evaporation under reduced pressure was purified by column chromatography (CH_2Cl_2 : acetone, 1:0 to 4:1, followed by CH_2Cl_2 : MeOH 95:5 to 75:15) to obtain compound **32**. Product **33** was also obtained as a side product (oxyrane ring opening instead of the typical SN_2 reaction to the carbon linked to the chlorine atom), in a 3:1 ratio.

(*S,E*)-2-(4-oxyranphenyl)-5-hydroxy-7-methoxy-2,3-dihydrochromen-4-one (**32**). Amorphous yellow power (180 mg, 75% yield). ^{1}H NMR (300 MHz, Acetone-D6) δ = 7.49 (d, *J* = 8.7 Hz, 2 H), 7.03 (d, *J* = 8.7 Hz, 2 H), 6.06 (d, *J* = 2.3 Hz, 1 H), 6.04 (d, *J* = 2.3 Hz, 1 H), 5.52 (dd, *J* = 12.8, 3.1 Hz, 1 H), 4.37 (dd, *J* = 11.3, 3.7 Hz, 1 H), 3.90 (dd, *J* = 11.3, 6.4 Hz, 1 H), 3.84 (s, 3 H), 3.33 (ddt, 6.4, 3.7, 2.6 Hz, 1 H), 3.21 (dd, *J* = 17.1, 12.8 Hz, 1 H), 2.85 (dd, *J* = 6.4, 3.7 Hz, 1 H), 2.79 (dd, *J* = 17.1, 3.1 Hz, 1 H), 2.72 (dd, *J* = 6.4, 2.6 Hz, 1 H); ^{13}C NMR (75 MHz, Acetone-D6) δ = 197.5, 168.9, 165.0, 164.1, 160.0, 132.3, 129.0, 115.5, 103.8, 95.5, 94.6, 79.8, 70.2, 56.3, 50.6, 44.4, 43.5 ppm. LRMS (ESI) *m/z* (positive mode) 379 [*M* + K]$^+$.

(*S,E*)-2-[4-(3-chloro-2-hydroxypropoxy)phenyl]-5-hydroxy-7-methoxy-2,3-dihydrochromen-4-one (**33**). Amorphous yellow powder (66 mg, 25% yield). ^{1}H NMR (300 MHz, Acetone-D6) δ = 7.48 (d, *J* = 8.5 Hz, 2 H), 7.03 (d, *J* = 8.5 Hz, 2 H), 6.05 (d, *J* = 2.3 Hz, 1 H), 6.03 (d, *J* = 2.3 Hz, 1 H), 5.49 (dd, *J* = 12.8, 3.1 Hz, 1 H), 4.22 (m, 1 H), 4.13 (dd, *J* = 5.2, 0.8 Hz, 2 H), 3.84 (s, 3 H), 3.83 (dd, *J* = 11.2, 5.2 Hz, 1 H), 3.74 (dd, *J* = 11.2, 5.2, 1 H), 3.18 (dd, *J* = 17.1, 12.8 Hz, 1 H), 2.77 (dd, *J* = 17.1, 3.1 Hz, 1 H); ^{13}C NMR (75 MHz, Acetone-D6) δ = 197.4, 168.8, 164.9, 164.0, 159.9, 132.1, 128.8, 115.4, 103.7, 95.5, 94.6, 79.7, 70.4, 70.0, 56.2, 47.1, 43.4 ppm. LRMS (ESI) *m/z* (positive mode) 416 [*M* + H]$^+$.

4.1.6. General preparation of compounds 34-39.

To 20 mg (1 equiv.) of compound **32** dissolved in MeOH was added 1equiv. of the chosen amine and a catalytic amount of acetic acid (0.01 equiv.). The mixture was stirred under reflux for 24-48 h. The reaction mixture was evaporated under vacuum at 40 ºC and extracted with ethyl acetate. The organic layers were combined and dried (Na_2SO_4). The solvent was removed under vacuum at 40 ºC and the obtained residue was purified by preparative TLC.

(*S,E*)-2-[4-(3-diethylamino-2-hydroxypropoxy)phenyl]-5-hydroxy-7-methoxy-2,3-dihydrochromen-4-one (**34**). Amorphous yellow powder, obtained from the reaction of compound **32** with diethylamine (15 mg, 63% yield). $[\alpha]_D^{20}$ + 8.4 ° (c 0.1, MeOH); ^{1}H NMR (300 MHz, acetone-D6-$CDCl_3$) δ = 7.38 (d, *J* = 8.8 Hz, 2 H), 6.94 (d, *J* = 8.8 Hz, 2 H), 5.99 (d, *J* = 2.4 Hz, 1 H), 5.98 (d, *J* = 2.4 Hz, 1 H), 5.39 (dd, *J* = 12.8, 3.0 Hz, 1 H), 3.97 (m, 3 H), 3.78 (s, 3 H), 3.08 (dd, *J* = 17.2, 12.8 Hz, 1 H), 2.73 (dd, *J* = 17.2, 3.0 Hz, 1 H), 2.66-2.48 (m, 6 H),

1.00 ... 8.9, CDCl3) δ = 196.4, 168.1, 164.3, 163.3, 159.6, 131.0, 128.0, 115.0, 103.2, 95.0, 94.1, 79.2, 71.0, 66.7, 55.7, 55.1, 47.6, 43.4, 12.0 ppm. LRMS (ESI) *m/z* (positive mode) 416 [M + H]$^+$.

(*S,E*)-2-{4-[2-hydroxy-(3-piperidin-1-yl)-propoxy]phenyl}-5-hydroxy-7-methoxy-2,3-dihydrochromen-4-one (**35**). Amorphous yellow powder, obtained from the reaction of compound **32** with piperidine (15 mg, 62% yield). ^{1}H NMR (300 MHz, $CDCl_3$) δ = 7.37 (d, J = 8.6 Hz, 2 H), 6.97 (d, J = 8.6 Hz, 2 H), 6.07 (d, J = 2.3 Hz, 2 H), 6.04 (d, J = 2.3 Hz, 2 H), 5.36 (dd, J = 13.0, 3.0 Hz, 1 H), 4.08 (tdd, J = 10.3, 6.7, 4.1 Hz, 1 H), 4.00 (m, 1 H), 3.99 (d, J = 0.8 Hz, 1 H), 3.80 (s, 3H), 3.04 (dd, J = 17.2, 13.0 Hz, 1 H), 2.78 (dd, J = 17.2, 3.0 Hz, 1 H), 2.49 (d, J = 2.5 Hz, 1 H), 2.47 (s, 1 H), 2.68-2.56 (m, 2 H), 2.43-2.23 (m, 2 H), 1.66-1.54 (m, 4 H), 1.47 (hex, J = 5.7 Hz, 2 H); ^{13}C NMR (75 MHz, $CDCl_3$) δ = 196.2, 168.1, 164.2, 163.0, 159.4, 130.7, 127.8, 115.0, 103.3, 95.2, 94.4, 79.1, 70.7, 65.4, 55.8, 55.2, 54.8, 43.3, 26.2, 24.3 ppm. LRMS (ESI) *m/z* (positive mode) 428 [M + H]$^+$.

(*S,E*)-2-[Methyl 2-hydroxy-(3-piperidine-4-carboxylate) propoxy]-5-hydroxy-7-methoxy-2,3-dihydrochromen-4-one (**36**). Amorphous yellow powder, isolated after the reaction of compound **32** with methyl 2-hydroxy-3-piperidine-4-carboxylate (14 mg, 53% yield). $[\alpha]_D^{20}$ – 7.0 ° (c 0.1, MeOH); ^{1}H NMR (300 MHz, Acetone-D6) δ = 7.49 (d, J = 8.6 Hz, 2 H), 7.02 (d, J = 8.6 Hz, 2 H), 6.06 (d, J = 2.3 Hz, 1 H), 6.04 (d, J = 2.3 Hz, 1 H), 5.53 (dd, J = 13.0, 3.0 Hz, 1 H), 4.10 – 4.05 (m, 3 H), 3.85 (s, 3 H), 3.62 (s, 3H), 3.23 (dd, J = 17.2, 13.0 Hz, 1 H), 2.78 (dd, J = 17.2, 3.0 Hz, 1 H), 2.50 (dt, J = 12.6, 5.5 Hz, 1 H), 2.32 (m, 1 H), 2.22 (td, J = 11.4, 10.7, 2.3 Hz, 1 H), 2.90 - 2.80 (m, 4 H), 1.86-1.79 (m, 2 H), 1.77-1.62 (m, 2 H); ^{13}C NMR (75 MHz, Acetone-D6) δ = 196.7, 174.8, 167.8, 164.1, 163.2, 161.5, 130.6, 128.1, 114.6, 102.8, 94.6, 93.7, 79.0, 71.1, 64.3, 61.6, 55.4, 53.8, 42.3, 40.6, 28.6 ppm. LRMS (ESI) *m/z* (positive mode) 486 [M + H]$^+$.

(*S,E*)-2-{4-[2-hydroxy-3-(1-benzylpiperidin-4-yl)-amino]propoxyphenyl}-5-hydroxy-7-methoxy-2,3-dihydrochromen-4-one (**37**). Amorphous yellow powder, obtained from the reaction of compound **32** with *N*-benzyl-4-aminopiperidine (14 mg, 46% yield). $[\alpha]_D^{20}$ + 3.8 ° (c 0.1, MeOH). ^{1}H NMR (300 MHz, Acetone-D6-$CDCl_3$) δ = 7.47 (d, J = 8.6 Hz, 2 H), 7.40 – 7.18 (m, 5 H), (d, J = 8.6 Hz, 2 H), 5.91 (d, J = 2.4 Hz, 2 H), 5.80 (d, J = 2.4 Hz, 2 H), 5.18 (dd, J = 12.2, 2.9 Hz, 1 H), 4.20 (dt, J = 10.2, 5.2 Hz, 1 H), 4.14 (s, 1 H), 4.12 (d, J = 0.9 Hz, 1 H), 3.86 – 3.70 (m, 3 H), 3.77 (s, 3 H), 3.50 (s, 2 H), 3.29 (dd, J = 16.8, 2.9 Hz, 1 H), 2.97 (dd, J = 16.8, 12.2 Hz, 1 H), 2.85 - 2.67 (m, 4 H), 1.98 - 1.56 (m, 4 H); ^{13}C NMR (75 MHz, Acetone-D6 - $CDCl_3$) δ = 169.9, 165.9, 165.8, 160.7, 159.8, 139.9, 133.2, 129.5, 129.0, 128.9, 127.7, 115.4, 101.3, 96.3, 92.4, 77.7, 70.4, 70.1, 55.6, 55.5, 52.2, 47.1, 33.7, 33.5 ppm. LRMS (ESI) *m/z* (positive mode) 533 [M + H]$^+$.

(*S,E*)-2-{4-[2-hydroxy-3-(1H-indol-1-yl)-propoxy]phenyl}-5-hydroxy-7-methoxy-2,3-dihydrochromen-4-one (**38**). Amorphous yellow powder, obtained from the reaction of compound **32** with indole (15 mg, 58% yield). ^{1}H NMR (300 MHz, Acetone-D6) δ = 7.56 (d, J = 7.8 Hz, 1 H), 7.50 (d, J = 8.7 Hz, 2 H), 7.42 (dd, J = 7.0, 1.0 Hz, 1 H), 7.09 (td, J = 7.0, 1.0 Hz, 1 H), 7.04 (d, J = 8.7 Hz, 2 H), 7.04 (dd, J = 7.0, 2.1 Hz, 1 H), 6.99 (td, J = 7.0, 1.0 Hz, 1 H), 6.06 (d, J = 2.3 Hz, 1 H), 6.04 (d, J = 2.5 Hz, 1 H), 5.53 (dd, J = 12.8, 3.0 Hz, 1 H), 4.21 (hept, J = 5.0 Hz, 1 H), 4.14 (s, 1 H), 4.12 (d, J = 0.9 Hz, 1 H), 3.77 (m, 2 H), 3.22 (dd, J = 17.1, 12.8 Hz, 1 H), 2.79 (dd, J = 17.1, 3.0 Hz, 1 H); ^{13}C NMR (75 MHz, Acetone-D6) δ = 125.5, 122.0, 121.0, 119.8, 115.4, 112.1, 103.7, 102.3, 95.4, 94.6, 79.8, 70.4, 70.0, 56.2, 47.1, 43.5 ppm. LRMS (ESI) *m/z* (positive mode) 482 [M + Na]$^+$.

(*S,E*)-2-{4-[2-hydroxy-3-(phenylsulphanyl)propoxy]phenyl}-5-hydroxy-7-methoxy-2,3-dihydrochromen-4-one (**39**). Amorphous white powder, obtained by reacting compound **32** with thiophenol (24 mg, 97% yield). ^{1}H NMR (300 MHz, Acetone-D6) δ = 7.55 (d, J = 8.6 Hz, 2 H), 7.50 (dd, J = 8.7, 2.1 Hz, 2 H), 7.38 (td, J = 7.4, 1.6 Hz, 2 H), 7.29 (dd, J = 7.3, 2.4 Hz, 1 H), 7.04 (d, J = 8.8 Hz, 2 H), 6.06 (d, J = 2.3 Hz, 2 H), 6.05 (d, J = 2.5 Hz, 1 H), 5.53 (dd, J = 12.8, 3.0 Hz, 1 H), 4.20 (dq, J = 9.0, 4.8, 4.1 Hz, 1 H), 4.14 (s, 1 H), 4.12 (d, J = 1.0 Hz, 1 H), 3.80 (dd, J = 11.7, 5.3 Hz, 2 H), 3.22 (dd, J = 17.1, 12.8 Hz, 1 H), 2.79 (dd, J = 17.1, 3.0 Hz, 1 H); ^{13}C NMR (75 MHz, Acetone-D6) δ = 196.2, 168.8, 164.2, 164.0, 160.0, 137.3, 132.2, 130.2, 128.9, 128.3, 128.2, 115.2, 103.7, 95.4, 94.6, 79.8, 70.4, 70.0, 56.2, 47.1, 43.4 ppm. LRMS (ESI) *m/z* (positive mode) 453 [M + H]$^+$.

4.2. Cell lines and cultures.

L5178Y mouse T-lymphoma cell (ECACC cat. no. 87111908, U.S. FDA, Silver Springs, MD, USA) were transfected with the pHa MDR1/A retrovirus[36] and the ABCB1 overexpressing cell line was further selected by supplementing the growth medium with colchicine (60 ng/mL) to maintain the MDR phenotype expression. Parental (L5178Y-PAR) and MDR (L5178Y-MDR) cells were cultivated in McCoy's 5A, supplemented with 10% heat-inactivated horse serum, 100 mg/L of a penicillin-streptomycin mixture and 100 U/L of L-glutamine and (Sigma-Aldrich Chemie GmbH, Steinheim, Germany). All cell lines were incubated in a humidified atmosphere (5% CO_2, 95% air) at 37 ºC.

4.3. Cytotoxicity assays

The cytotoxicity of compounds **1-39** was assessed in a range of decreasing concentrations (2-fold dilutions) in *ABCB1*-transfected mouse T-lymphoma cell lines (L5178Y-PAR and L5178Y-MDR). Cells were distributed into 96-well flat bottom microtiter plates in 100 µL of medium per well at a concentration of 1 x 10^4 per well, except for medium and cell control wells. All compounds were tested in duplicates with a maximum concentration of 100 µM. The microtiter plates were then incubated for 24 h, after which 20 µL of a 5 mg/mL MTT solution in phosphate-saline buffer (PBS) was added to each well (thiazolyl blue tetrazolium bromide, Sigma-Aldrich Chemie GmbH, Steinheim, Germany) and the plates were further incubated for another 4 hours. Next, 100 µL of SDS (sodium dodecyl sulfate, 10% in 0.01 M HCl solution) was added to each well and incubated overnight at 37 °C. Cell growth was determined by measuring optical density (OD) at 550 nm (ref. 630 nm) in a Multiscan EX ELISA reader (Thermo Labsystems, Cheshire, WA, USA). The percentage of inhibition of cell growth was determined according to the equation

$$100 - \left[\frac{\mathrm{OD_{sample}} - \mathrm{OD_{medium\ control}}}{\mathrm{OD_{cell\ control}} - \mathrm{OD_{medium\ control}}}\right] \times 100$$

The results were expressed as the mean ± SD, and the IC_{50} values were obtained by best fitting the dose-dependent inhibition curves independently in Libreoffice Calc and in GraphPad Prism 5.03 for Windows software.[37,38]

4.4. Rhodamine-123 (R123) accumulation assay.

resuspended in a serum-free McCoy's 5A medium and distributed in 500 µL aliquots in Eppendorf centrifuge tubes. All test compounds were added at 2.0 and 20 µM, verapamil at 20 µM (positive control, EGIS Pharmaceuticals PLC, Budapest, Hungary) and DMSO at 2% as solvent control. The samples were incubated at room temperature for 10 min, after which 10 µL (5.2 µM final concentration) of R123 was added and further incubated for 20 min at 37 °C. The samples were washed twice, resuspended in 1 mL PBS and analyzed by flow cytometry (Partec CyFlow® Space instrument, Partec GmbH, Münster, Germany). Histograms were evaluated regarding mean fluorescence intensity (FL-1), standard deviation and both FSC and SSC parameters. The fluorescence activity ratio (FAR) was calculated as the quotient between FL-1 of treated/untreated resistant cell line (L5178Y-MDR) over treated/untreated sensitive cell line (L5178Y-PAR), according to the following equation

$$\mathrm{FAR} = \frac{\mathrm{FL} - 1^{\mathrm{MDR}}_{\mathrm{treated}} / \mathrm{FL} - 1^{\mathrm{MDR}}_{\mathrm{untreated}}}{\mathrm{FL} - 1^{\mathrm{PAR}}_{\mathrm{treated}} / \mathrm{FL} - 1^{\mathrm{PAR}}_{\mathrm{untreated}}}$$

4.5. Drug combination assay.

The combination studies were designed as suggested in the CalcuSyn manual (http://www.biosoft.com), using a fixed ratio of compounds across a concentration gradient. The dilution of doxorubicin was performed horizontally (14.7 – 0.1 µM) while the dilutions of the MDR-reversal agent (at 2-fold of their IC_{50}'s) vertically in a microtiter plate to a final volume of 200 µL per well. The cells were distributed in 100 µL into wells in a concentration of 2 x 105 /mL and the plates were incubated for 48 h. Cell growth was determined after MTT staining, as previously described. Drug interactions were assessed according to Chou[12,13] using the CompuSyn v1.0 software. Each dose-response curve (individual agents as well as combinations) was linearly fitted to the median effect equation as a way to obtain the median effect value (thus corresponding to the IC_{50}) and slope (m). Goodness-of-fit was assessed using the linear correlation coefficient *r* and only data with $r > 0.90$ was considered. Combination index (CI) values are represented as the mean of three CI values calculated from different drug ratios ± standard deviation (SD) of the mean, for an inhibitory concentration of 50 % (IC_{50}). The extent of interaction between drugs was expressed using CI for mutually exclusive drugs. A CI close to 1 indicates additivity; $CI < 1$ defines synergism and $CI > 1$ is related to antagonism.

4.6. Molecular docking.

Molecular docking was performed using a previously refined murine P-glycoprotein,[14] derived from the original crystallographic data, comprising 100% identity between mouse and human structures for the residues inside the DBP. The final model used for docking can be downloaded from www.chemistrybits.com. Validation of the docking protocol was done by comparing the top-ranked docking pose of taxol with the data obtained for the taxol-bound human P-gp, recently obtained by cryo-EM [39] (Figure S61). MarvinSketch 17.24.0 was used for drawing structures. All ligands were exported to MOE, minimized with the MMFF94x force-field (adjusting hydrogen and lone pairs by default) and exported again in mol2 format to further obtain PDBQT files with AutoDockTools[40] for utilization in AutoDock VINA 1.1.2..[41] Two binding locations were defined: i) a docking box including the whole internal cavity and in agreement with our dimensions *xyz* of 35.25 × 25.50 × 45.25 Å respectively (*xy* corresponds to the membrane plane), and ii) two docking boxes comprising the ATP-binding site at each nucleotide-binding domain, centered at the Walker A motif and with dimensions *xyz* of 10.68 × 10.68 × 10.68 Å respectively. Due to the large search space volumes of the defined docking boxes, 'exhaustiveness' parameter was set to 50. Visual inspection of the docking poses was made using MOE to identify individual docking zones and binding modes. Identification of binding residues, hydrogen bonding and cross-interaction capability (CIc) of compounds were evaluated using Ligplot [42] and in-house python scripts.

4.7. Molecular dynamics simulations.

From a previous study a system comprising P-gp inserted in a POPC bilayer patch was used.[15] Ligand molecules were parameterized with the 54a7[43,44] parameter set of GROMOS96 [45] force-field in PRODRG[46] server, with AM1-BCC partial charges calculated in MOE v2019.01,[47] in agreement with available literature.[48] The GROMACS 2020.1 simulation package[49] was used for all MD simulations. All simulations were performed as previously published.[15,27,50]

4.8. Data analysis.

Concerning analysis, the last 30-ns of each 50-ns MD run were considered as production. Hydrogen bonds were estimated using *gmx hbond*[51] and non-bonded contacts with *g_contacts*[52] tools. Relative free-energies of binding were obtained with *g_mmpbsa* (ΔG_{bind})[53], and as P-gp is inserted in a membrane, a correction to the polar solvation energies must be taken as previously described.[50] Ligand efficiency (LE) was obtained from the ratio between the number of protein−ligand contacts with frequencies greater than 0.50 and the total number of protein−ligand contacts, calculated with *g_contacts*. The compounds' cross-interaction capability (CIc) was calculated as the ratio between the number of hydrogen-bond and non-bonded interactions observed between each molecule and P-gp's N-terminal and C-terminal halves, exclusively at the M-site. Weak, <50%; Moderate, < 75%; Strong, > 75%.

Acknowledgments

We acknowledge the European Structural & Investment Funds through the COMPETE Programme and National Funds through FCT, Fundação para a Ciência e a Tecnologia (FCT, Portugal), under the projects PTDC/MED-QUI/30591/2017, FCT/NKFIH (2019/2020) and SAICT-PAC/0019/2015. The study was also supported by the project GINOP-2.3.2-15-2016-00012. R.J.F. acknowledges FCT for the Ph.D. grant SFRH/BD/84285/2012. We also thank COST Action CA17104 STRATAGEM.

References

1. Food and Drug Administration. *In Vitro Metabolism- and Transporter- Mediated Drug-Drug Interaction Studies*. Food and Drug Administration; 2017:1-47.
2. Gottesman MM. Mechanisms of cancer drug resistance. *Annu Rev Med*. 2002;53:615-627. doi:10.1146/annurev.med.53.082901.103929
3. Tsuruo T, Lida H, Tsukagoshi S, Sakurai Y. Overcoming of Vincristine Resistance in P388 Leukemia in Vivo and in Vitro through Enhanced Cytotoxicity of Vincristine and Vinblastine by Verapamil. *Cancer Res*. 1981;41(5):1967-1972.

multidrug resistance: insights into the efflux by ABC transports from in silico studies. *WIREs Comput Mol Sci*. 2015;5(1):27-55. doi:10.1002/wcms.1196
5. Eckford PDW, Sharom FJ. ABC efflux pump-based resistance to chemotherapy drugs. *Chem Rev*. 2009;109(7):2989-3011. doi:10.1021/cr9000226
6. Ferreira MJU, Duarte N, Reis M, Madureira AM, Molnár J. Euphorbia and Momordica metabolites for overcoming multidrug resistance. *Phytochem Rev*. 2014;13(4):915-935. doi:10.1007/s11101-014-9342-8
7. Ferreira RJ, Baptista R, Moreno A, et al. Optimizing the flavanone core toward new selective nitrogen-containing modulators of ABC transporters. *Future Med Chem*. 2018;10(7):725-741. doi:10.4155/fmc-2017-0228
8. Chiba P, Hitzler M, Richter E, et al. Studies on Propafenone-type Modulators of Multidrug Resistance III: Variations on the Nitrogen. *Quant Struct-Act Relat*. 1997;16(5):361-366. doi:10.1002/qsar.19970160502
9. Chiba P, Burghofer S, Richter E, Tell B, Moser A, Ecker G. Synthesis, Pharmacologic Activity, and Structure-Activity Relationships of a Series of Propafenone-Related Modulators of Multidrug Resistance. *J Med Chem*. 1995;38(14):2789-2793. doi:10.1021/jm00014a031
10. Zamora JM, Pearce HL, Beck WT. Physical-chemical properties shared by compounds that modulate multidrug resistance in human leukemic cells. *Mol Pharmacol*. 1988;33(4):454-462.
11. Ferreira RJ, Ferreira MJU, dos Santos DJVA. Do Drugs Have Access to the P-Glycoprotein Drug-Binding Pocket through Gates? *J Chem Theory Comput*. 2015;11(10):4525-4529. doi:10.1021/acs.jctc.5b00652
12. Chou T-C. Drug Combination Studies and Their Synergy Quantification Using the Chou-Talalay Method. *Cancer Res*. 2010;70(2):440-446. doi:10.1158/0008-5472.CAN-09-1947
13. Chou T-C. Theoretical Basis, Experimental Design, and Computerized Simulation of Synergism and Antagonism in Drug Combination Studies. *Pharmacol Rev*. 2006;58(3):621-681. doi:10.1124/pr.58.3.10
14. Ferreira RJ, Ferreira MJU, dos Santos DJVA. Molecular docking characterizes substrate-binding sites and efflux modulation mechanisms within P-glycoprotein. *J Chem Inf Model*. 2013;53(7):1747-1760. doi:10.1021/ci400195v
15. Ferreira RJ, Ferreira MJU, Santos DJVA dos. Insights on P-Glycoprotein's Efflux Mechanism Obtained by Molecular Dynamics Simulations. *J Chem Theory Comput*. 2012;8(6):1853-1864. doi:10.1021/ct300083m
16. Kim JY, Henrichs S, Bailly A, et al. Identification of an ABCB/P-glycoprotein-specific inhibitor of auxin transport by chemical genomics. *J Biol Chem*. 2010;285(30):23309-23317. doi:10.1074/jbc.M110.105981
17. Borchers C, Boer R, Klemm K, et al. Characterization of the Dexniguldipine Binding Site in the Multidrug Resistance-Related Transport Protein P-Glycoprotein by Photoaffinity Labeling and Mass Spectrometry. *Mol Pharmacol*. 2002;61(6):1366-1376. doi:10/b5bmcf
18. Isenberg B, Thole H, Tümmler B, Demmer A. Identification and localization of three photobinding sites of iodoarylazidoprazosin in hamster P-glycoprotein. *Eur J Biochem*. 2001;268(9):2629-2634. doi:10.1046/j.1432-1327.2001.02155.x
19. Conseil G, Baubichon-Cortay H, Dayan G, Jault J-M, Barron D, Di Pietro A. Flavonoids: A class of modulators with bifunctional interactions at vicinal ATP- and steroid-binding sites on mouse P-glycoprotein. *Proc Natl Acad Sci U A*. 1998;95(17):9831-9836.
20. Loo TW, Clarke DM. P-glycoprotein ATPase activity requires lipids to activate a switch at the first transmission interface. *Biochem Biophys Res Commun*. 2016;472(2):379-383. doi:10.1016/j.bbrc.2016.02.124
21. Loo TW, Clarke DM. The Transmission Interfaces Contribute Asymmetrically to the Assembly and Activity of Human P-glycoprotein. *J Biol Chem*. 2015;290(27):16954-16963. doi:10.1074/jbc.M115.652602
22. Loo TW, Clarke DM. Locking Intracellular Helices 2 and 3 Together Inactivates Human P-glycoprotein. *J Biol Chem*. 2014;289(1):229-236. doi:10.1074/jbc.M113.527804
23. Saija A, Bonina F, Trombetta D, et al. Flavonoid-biomembrane interactions: A calorimetric study on 1995;124(1):1-8. doi:10.1016/0378-5173(95)00051-5
24. Walle T, Ta N, Kawamori T, Wen X, Tsuji PA, Walle UK. Cancer chemopreventive properties of orally bioavailable flavonoids—Methylated versus unmethylated flavones. *Biochem Pharmacol*. 2007;73(9):1288-1296. doi:10.1016/j.bcp.2006.12.028
25. Lomize AL, Hage JM, Schnitzer K, et al. PerMM: A Web Tool and Database for Analysis of Passive Membrane Permeability and Translocation Pathways of Bioactive Molecules. *J Chem Inf Model*. 2019;59(7):3094-3099. doi:10/ggm6f6
26. Lomize AL, Pogozheva ID. Physics-Based Method for Modeling Passive Membrane Permeability and Translocation Pathways of Bioactive Molecules. *J Chem Inf Model*. 2019;59(7):3198-3213. doi:10/ggm6f5
27. Isca VMS, Ferreira RJ, Garcia C, et al. Molecular Docking Studies of Royleanone Diterpenoids from Plectranthus spp. as P-Glycoprotein Inhibitors. *ACS Med Chem Lett*. 2020;11(5):839-845. doi:10.1021/acsmedchemlett.9b00642
28. Mollazadeh S, Hadizadeh F, Ferreira RJ. Theoretical studies on 1,4-dihydropyridine derivatives as P-glycoprotein allosteric inhibitors: insights on symmetry and stereochemistry. *J Biomol Struct Dyn*. Published online June 23, 2020:1-12. doi:10/gg227z
29. Aller SG, Yu J, Ward A, et al. Structure of P-glycoprotein reveals a molecular basis for poly-specific drug binding. *Science*. 2009;323(5922):1718-1722. doi:10.1126/science.1168750
30. Loo TW, Clarke DM. Tariquidar inhibits P-glycoprotein drug efflux but activates ATPase activity by blocking transition to an open conformation. *Biochem Pharmacol*. 2014;92(4):558-566. doi:10.1016/j.bcp.2014.10.006
31. Loo TW, Clarke DM. Mapping the Binding Site of the Inhibitor Tariquidar That Stabilizes the First Transmembrane Domain of P-glycoprotein. *J Biol Chem*. 2015;290(49):29389-29401. doi:10.1074/jbc.M115.695171
32. Shapiro AB, Ling V. Transport of LDS-751 from the cytoplasmic leaflet of the plasma membrane by the rhodamine-123-selective site of P-glycoprotein. *Eur J Biochem*. 1998;254(1):181-188. doi:10.1046/j.1432-1327.1998.2540181.x
33. Ferreira RJ, dos Santos DJVA, Ferreira MJU. P-glycoprotein and membrane roles in multidrug resistance. *Future Med Chem*. 2015;7(7):929-946. doi:10.4155/fmc.15.36
34. Nervi P, Li-Blatter X, Aänismaa P, Seelig A. P-glycoprotein substrate transport assessed by comparing cellular and vesicular ATPase activity. *Biochim Biophys Acta*. 2010;1798(3):515-525. doi:10.1016/j.bbamem.2009.11.022
35. Loo TW, Clarke DM. Drugs Modulate Interactions between the First Nucleotide-Binding Domain and the Fourth Cytoplasmic Loop of Human P-Glycoprotein. *Biochemistry*. 2016;55(20):2817-2820. doi:10.1021/acs.biochem.6b00233
36. Pastan I, Gottesman MM, Ueda K, Lovelace E, Rutherford AV, Willingham MC. A retrovirus carrying an MDR1 cDNA confers multidrug resistance and polarized expression of P-glycoprotein in MDCK cells. *Proc Natl Acad Sci U A*. 1988;85(12):4486-4490. doi:10.1073/pnas.85.12.4486
37. *Graphpad Prism*. GraphPad Software; 2015. www.graphpad.com
38. Motulsky H, Hristopoulos A. *Fitting Models to Biological Data Using Linear and Nonlinear Regression: A Practical Guide to Curve Fitting*. Oxford University Press; 2004.
39. Alam A, Kowal J, Broude E, Roninson I, Locher KP. Structural insight into substrate and inhibitor discrimination by human P-glycoprotein. *Science*. 2019;363(6428):753-756. doi:10.1126/science.aav7102
40. Morris GM, Huey R, Lindstrom W, et al. AutoDock4 and AutoDockTools4: Automated docking with selective receptor flexibility. *J Comput Chem*. 2009;30(16):2785-2791. doi:10.1002/jcc.21256
41. Trott O, Olson AJ. AutoDock Vina: improving the speed and accuracy of docking with a new scoring function, efficient optimization, and multithreading. *J Comput Chem*. 2010;31(2):455-461. doi:10.1002/jcc.21334
42. Wallace AC, Laskowski RA, Thornton JM. LIGPLOT: a program to generate schematic diagrams of protein-ligand interactions. *Protein Eng*. 1995;8(2):127-134. doi:10.1093/protein/8.2.127
43. Reif MM, Winger M, Oostenbrink C. Testing of the GROMOS Force-Field Parameter Set 54A8: Structural Properties of Electrolyte Solutions, Lipid Bilayers, and Proteins. *J Chem*

2013;1301291353935000. doi:10.1021/ci500874c
44. Schmid N, Eichenberger AP, Choutko A, et al. Definition and testing of the GROMOS force-field versions 54A7 and 54B7. *Eur Biophys J*. 2011;40(7):843-856. doi:10.1007/s00249-011-0700-9
45. Schuler LD, Daura X, Van Gunsteren WF. An improved GROMOS96 force field for aliphatic hydrocarbons in the condensed phase. *J Comput Chem*. 2001;22:1205-1218. doi:10.1063/1.3605302
46. Schüttelkopf AW, van Aalten DMF. PRODRG: a tool for high-throughput crystallography of protein-ligand complexes. *Acta Crystallogr Biol Crystallogr*. 2004;60(Pt 8):1355-1363. doi:10.1107/S0907444904011679
47. *Molecular Operating Environment (MOE) V2019.01*. Chemical Computing Group Inc; 2019.
48. Lemkul JA, Allen WJ, Bevan DR. Practical considerations for building GROMOS-compatible small-molecule topologies. *J Chem Inf Model*. 2010;50(12):2221-2235. doi:10.1021/ci100335w
49. Pronk S, Páll S, Schulz R, et al. GROMACS 4.5: a high-throughput and highly parallel open source molecular simulation toolkit. *Bioinformatics*. 2013;29(7):845-854. doi:10.1093/bioinformatics/btt055
50. Ferreira RJ, Ferreira MJU, dos Santos DJVA. Do adsorbed drugs onto P-glycoprotein influence its efflux capability? *Phys Chem Chem Phys*. 2015;17(34):22023-22034. doi:10.1039/C5CP03216D
51. van der Spoel D, van Maaren PJ, Larsson P, Tîmneanu N. Thermodynamics of hydrogen bonding in hydrophilic and hydrophobic media. *J Phys Chem B*. 2006;110(9):4393-4398. doi:10.1021/jp0572535
52. Blau C, Grubmuller H. g_contacts: Fast contact search in bio-molecular ensemble data. *Comput Phys Commun*. 2013;184(12):2856-2859. doi:10.1016/j.cpc.2013.07.018
53. Kumari R, Kumar R, Lynn A. g_mmpbsa —A GROMACS Tool for High-Throughput MM-PBSA Calculations. *J Chem Inf Model*. 2014;54(7):1951-1962. doi:10.1021/ci500020m

Supplementary Material

^{1}H and ^{13}C NMR spectra and structural elucidation of compounds. Cytotoxicity of compounds **1-39** on parental (L5178Y-PAR) and *ABCB1*-transfected (L5178Y-MDR) mouse T-lymphoma cells; Flow cytometry data for mouse T-lymphoma L5178Y PAR and MDR cells, verapamil (control), DMSO (control) and compounds **1-39**; Docking, membrane permeation and molecular dynamics results for compounds **1-39**.

Declaration of interests

☒ The authors declare that they have no known competing financial interests or personal relationships that could have appeared to influence the work reported in this paper.

☐The authors declare the following financial interests/personal relationships which may be considered as potential competing interests: